T.C.

MUĞLA SITKI KOÇMAN UNIVERSITY

GRADUATE SCHOOL OF NATURAL AND APPLIED SCIENCES

DEPARTMENT OF GEOLOGICAL ENGINEERING

QUANTIFICATION OF HEAT AND WATER FLUXES AT 2-D REACH SCALE WITH FIBER OPTIC DISTRIBUTED SENSING: AVENELLES BASIN

MASTER THESIS

DENİZ KILIÇ

SEPTEMBER 2018

MUĞLA

DENİZ KILIÇ DEPARTMENT OF GEOLOGICAL ENGINEERING MASTER THESIS MUĞLA 2018

T.C.

MUĞLA SITKI KOÇMAN UNIVERSITY

GRADUATE SCHOOL OF NATURAL AND APPLIED SCIENCES

DEPARTMENT OF GEOLOGICAL ENGINEERING

QUANTIFICATION OF HEAT AND WATER FLUXES AT 2-D REACH SCALE WITH FIBER OPTIC DISTRIBUTED SENSING: AVENELLES BASIN

MASTER THESIS

DENİZ KILIÇ

SEPTEMBER 2018

MUĞLA

MUGLA SITKI KOCMAN UNIVERSITY

Graduate School of Natural and Applied Sciences

THESIS CONFIRMATION

The thesis, prepared by **DENİZ KILIC,** titled as **"QUANTIFICATION OF HEAT AND WATER FLUXES AT 2-D REACH SCALE WITH FIBER OPTIC DISTRIBUTED SENSING: AVENELLES BASIN"** has been accepted unanimously/majority by the jury listed below that fulfils the necessary conditions for master degree of Department of Geological Engineering at 17/09/2018.

THESIS DEFENCE JURY

Prof. Dr. Moumtaz RAZACK **(Head of Jury)**
Department of Geosciences,
University of Poitiers, Poitiers, France
Signature:

Assoc. Prof. Dr. Bedri KURTULUŞ **(Supervisor)**
Department of Geological Engineering,
Mugla Sitki Kocman University, Muğla
Signature:

Asst. Prof. Dr. Jacques BODIN **(Member)**
Department of Geosciences,
University of Poitiers, Poitiers, France
Signature:

Asst. Prof. Dr. Nicolas FLIPO **(Member)**
Department of Geosciences,
Mines ParisTech, Paris, France
Signature:

Asst. Prof. Dr. Can CANOGLU **(Member)**
Department of Environmental Engineering,
Sinop University, Sinop
Signature:

Date of Defence: 17/09/2018

MUGLA SITKI KOCMAN UNIVERSITY

Graduate School of Natural and Applied Sciences

THESIS CONFIRMATION

The thesis, prepared by **Deniz KILIC,** titled as **"QUANTIFICATION OF HEAT AND WATER FLUXES AT 2-D REACH SCALE WITH FIBER OPTIC DISTRIBUTED SENSING: AVENELLES BASIN"** has been accepted unanimously/majority by the jury listed below that fulfils the necessary conditions for master degree of Department of Geological Engineering at 17/09/2018.

DEPARTMENT CONFIRMATION

Prof. Dr. Murat GUL — Signature:

Head of Department of Geological Engineering,
Mugla Sitki Kocman University, Muğla

Assoc. Prof. Dr. Bedri KURTULUŞ — Signature:

Supervisor, Department of Geological Engineering,
Mugla Sitki Kocman University, Muğla

Date of Defence: 17/09/2018

I proclaim that all the results, documents, information used are obtained by me during the research period. This thesis is prepared in compliance with the scientific and ethical rules. Moreover, during the research and reporting period, all the documents obtained by other agents are properly cited and their sources are given as a necessity of scientific and ethical rigor.

DENİZ KILIÇ

17/09/2018

To my family

ACKNOWLEDGEMENTS

This thesis is a result of the graduation research for the Master 2 studies in Hydrogeology and associated transfers at the faculty of Fundamental and Applied Sciences of University of Poitiers. The research was conducted at the Mines ParisTech in Paris-France. I would like to thank everyone in Mines ParisTech who greeted and helped me throughout my research.

I would like to thank to my supervisor Asst. Prof. Dr. Agnès Rivière for her guidance and feedback during my research and reporting process. I would like to thank my supervisor Assoc. Prof. Dr. Bedri Kurtulus for his support and guidance during my master studies and thesis research process.

I would like to thank Prof. Dr. Olivier Bour, Prof. Dr. Nicolas Flipo, and Nataline Simon for their valuable time and discussions about the hyporheic zone and fiber optic methods. Their feedback and suggestions were of great value for this thesis. I want to thank to Dr. Jonathan Schuite and Loic Marlot for their great help during the field excursion.

I am thankful to the Muğla Sıtkı Koçman Vakfı and Embassy of France in Turkey for the scholarship provided to me during my master's studies. This research is realized with the funding of Critex and PIREN-Seine. Therefore, I am grateful for the funding, so this study could be realized.

Finally, I would like to thank to my parents, and friends in France, Turkey for their support throughout my master's and research.

ÖZET

FİBER OPTİK YÖNTEMLERLE DERE VE YERALTI SULARININ ARASINDA GERCEKLEŞEN SU VE ENERJİ AKIŞININ MODELLENMESİ: AVENELLES HAVZASI

Deniz KILIÇ

Yüksek Lisans Tezi

Fen Bilimleri Enstitüsü

Jeoloji Mühendisliği Ana Bilim Dalı

Danışman: Doç. Dr. Bedri KURTULUŞ

İkinci (Ortak) Danışman: Dr. Öğr. Üyesi. Agnès RIVIERE

Eylül, 2018, 71 sayfa

Su kaynaklarına duyulan ihtiyacın artması ve doğadaki tahribatın gittikçe artması, su kaynaklarını yönetenleri ve bu konuda çalışanları koruyucu önlemler almaya itmiştir. Yer üstü sularının ve yer altı sularının birleştiği bölge olan hiporeik bölge ise geçtiğimiz yıllarda araştırmacılar tarafından oldukça ilgi çekmiştir. Hiporeik bölgenin su kaynaklarının kalitesi ve miktarı için olan önemi farklı skalalarda araştırmacılar tarafından oldukça iyi anlaşılmıştır. Fakat, hiporeik bölge (HZ) üzerinde alınacak kararlar açısından yeni ve güvenilir parametrelere ihtiyaç gittikçe artmaktadır. Bu tez su yönetimi açısından ihtiyaç duyulan parametreleri elde etmek için yeni bir yöntem ortaya koymakta ve su kaynakları yöneticilerine daha iyi karar alma mekanizması oluşturmayı hedeflemektedir. Bu çerçeve içinde, yeni bir izleme yöntemi olan fiber optik dağıtımlı sıcaklık izleme yöntemi (FO-DTS) ve yerel izleme istasyonu (mini-LOMOS) yöntemi birleştirilmiştir. Elde edilen veri, tam bağlaşık geçici sonlu bir su ve sıcaklık akış modeli ile çözümlenmiş ve hidro-termal parametreler inversiyon kodu ile tek boyutlu dikey model için elde edilmiştir. Fiber optik verisi, bağımsız sıcaklık verisiyle sağlaması yapılmış ve hiporeik bölge içinde 2 boyutlu bir sıcaklık ve su akış modeli geliştirilmiştir. Model performansı istatistiksel karşılaştırmayla ortaya konulmuştur. Kök ortalama kare hatası (RMSE), 0.24 olarak bulunmuş ve 2 boyutlu model ile gözlemlenen sıcaklıklar arasındaki fark 0.2°C olarak elde edilmiştir. Bu çalışmanın sonucunda, elde edilen model sayesinde, su kaynakları yönetimi ve çalışanları için daha güvenilir bir karar mekanizması elde edilmiştir.

Anahtar Kelimeler: Hiporeik Bölge, Avenelles, Isı ve Su Akış Modellemesi, Fiber Optik Dağıtımlı Sıcaklık İzleme, Su Kaynakları

ABSTRACT

QUANTIFICATION OF HEAT AND WATER FLUXES AT 2-D REACH SCALE WITH FIBER OPTIC DISTRIBUTED SENSING: AVENELLES BASIN

Deniz KILIÇ

Master of Science (M.Sc.)

Graduate School of Natural and Applied Sciences

Department of Geological Engineering

Supervisor: Assoc. Prof. Dr. Bedri KURTULUŞ

Co-supervisor: Asst. Prof. Dr. Agnès RIVIERE

September 2018, 71 pages

The growing water demand, increasing adverse effect of mankind to the nature forces water managers and researchers to take protective measures to protect the quality and quantity of the water. The interface between groundwater and surface water within river ecosystems, called hyporheic zone (HZ), gained attention from a range of disciplines. The importance of HZ for the quality and quantity of the water is well understood at local and reach scales. However, there is a need for a method to provide parameter sets to water managers regarding HZ to make decisions. This thesis attempts to provide a new method for estimation of parameters at reach scale for water managers and researchers, and better understanding of the effect of pool and riffle systems at local scale. For this purpose, novel monitoring tools fiber-optic distributed temperature sensing and mini-LOcal MOnitoring Station (LOMOS) are combined and processed with a fully coupled transient finite model solving the water flow and heat transport in porous media. The parameters are obtained with the help of an inversion script, and a 2-D mesh is developed to test the parameters that are obtained from 1-D vertical model for the HZ. The results are validated with independent observations for FO-DTS, observed temperature series for hydro-thermal parameters, and observed temperature series for 2-D mesh. The average RMSE is 0.24 for the parameters, and the difference between observed vs. simulated temperature time series is less than 0.2°C for 2-D mesh. The implications of these results are the method proposed here can pave the way for better decisions on HZ for water managers and researchers, and a better understanding of the effect of pool and riffle sequences.

Keywords: Hyporheic Zone, Avenelles, Heat and Water Flux Modeling, Fiber Optic Distributed Temperature Sensing, Water Resources

TABLE OF CONTENTS

LIST OF FIGURES

LIST OF TABLES

1. INTRODUCTION

1.1 Background

The increasing water demand, the degraded state of streams in terms of water quality, quantity, and the growing research on hyporheic zone (HZ) at reach scale requires collaborative efforts of water managers and researchers to practice most sustainable and effective management strategies to protect and provide water. In 2050, the global population is predicted to rise to about 9 billion people. To supply the needs of the growing population, 75% more water than we use today will be required (Chery and de Marsily, 2007). Providing this water while at the same time maintaining the quality of the water will be a tremendous task. Therefore, water resources are an ever-growing concern for both quality, and quantity as the supply is decreasing as result of human development and interference with the water resources. To cope with the challenges this demand has, a systemic view of the hydrological cycle emerged, which led to the concept of continental hydrosystem (Flipo et al., 2012; Flipo et al., 2014). In this context, a hydrosystem "is composed of storage components where water flows slowly (i.e. aquifers) and conductive components, where large quantities of water flow relatively quickly (i.e. surface water, rivers) (Flipo et al., 2012; Kurtulus et al., 2011).

In the interface of storage (i.e. aquifer) and conductive components (i.e. streams), lies a distinct zone called "hyporheic zone". This connection is particularly important because surface water is generally high in dissolved oxygen and nutrients, while groundwater tends to be low in dissolved oxygen and high in inorganic solutes. The mixing of surface water and groundwater creates a unique zone facilitating biogeochemical cycling, stream temperature buffering, pollutant attenuation, and enabling habitat growth (Boulton et al., 1998). Hyporheic zone is present throughout the stream-aquifer interface, hence it can be considered in different scales. Local scale is ranging between 10 cm - ≈ 10 m. Intermediate or reach scale is between ≈ 10 m - ≈ 1 km as in Figure 1.1. Catchment and watershed scale which connects the stream network to watershed, is ranging between ≈1 km - 10 km, and the hyporheic zone

exchanges are linked to the hydrological cycle and hydrogeological processes (Flipo et al., 2014). Recent studies state that complex multi-scale processes are taking place at the stream-aquifer interfaces (Poole et al., 2008). To understand these systems and their interactions, quantification of the exchange fluxes between groundwater and surface water is an important prerequisite for understanding and preserving quality of hydrosystems.

Hyporheic exchange of water and its constituents play an important role in fundamental hydrologic and ecologic processes both in rivers and subsurface aquifer such as discharge, moderation of water-level fluctuations, thermal buffering, biogeochemical reactions, transformation and retention of nutrients, pollutants, and its ecological effects (Hayashi and Rosenberry, 2002; Boano et al., 2014).

Temperature is a water quality key factor driving physical, chemical, and biological processes in aquatic and HZ ecosystems. It directly influences dissolved organic matter (solubility, saturation point, and content) dissolved oxygen concentrations, the solubility of other gases and solutes (weathering), and the speed of chemical and biological reactions. Moreover, it controls the metabolic rates, physiology, and life-history traits of aquatic organisms, of microinvertebrate (Allan and Ibañez Castillo, 2009; Boulêtreau et al., 2012; Poole and Berman, 2001; Mathers et al., 2017; Vieweg et al., 2016; Zheng, 2017). This explains that the need of accurate understanding of hyporheic zone temperatures has regained interest recently because of the threat of global climate change.

Although the dynamics of water fluxes between streams and aquifers are better understood, including the effect of hydrological events on flow reversal (Saleh et al., 2011; Flipo et al., 2014; Pryet et al., 2015; Baratelli et al., 2016), the state of connection processes of stream-aquifer systems (Rivière et al., 2014), as well as the bioclogging of the HZ (Newcomer et al., 2016), the relationship between water and heat fluxes still needs a better conceptualization. The temperature in the HZ depends on the climatic conditions, the hydrogeological context, and the porous medium properties. In other words, the temperature is mainly affected by the thermal and the hydraulic gradient between the stream and the aquifer. However, these gradients do not show a uniform pattern along the river channel. The flow between surface and groundwater follows complex dynamics (Flipo et al., 2014), in which upwelling and downwelling zones occur alternatively (White, 1990). Streambed topography (i.e.

riffle-pool sequence, steps, cascade), is the primary control of hyporheic exchange by generating sequences of downwelling and upwelling zones. In a riffle, surface water enters the HZ at the beginning of the riffle (downwelling zone) and returns to the stream at the end of it (upwelling zone)(Figure 1.1).

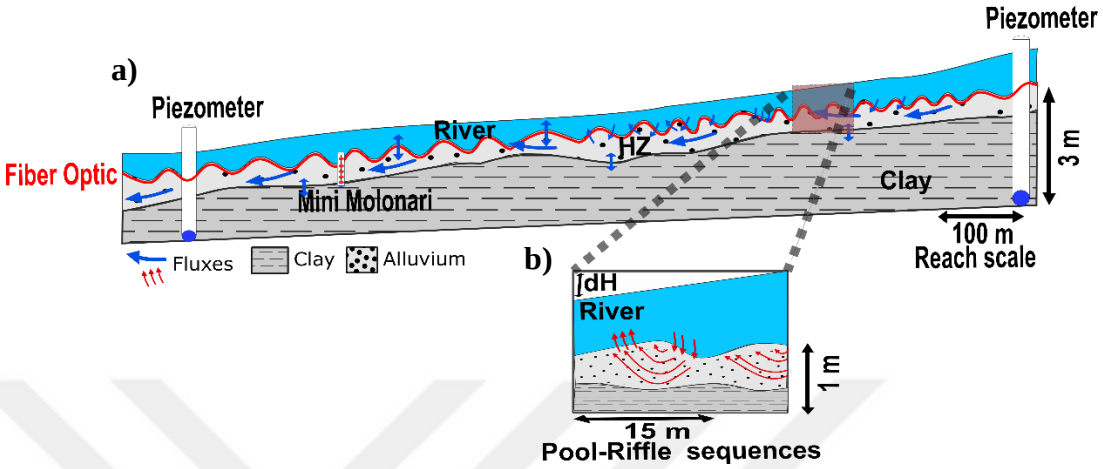

Figure 1.1: a) The conceptual hyporheic zone fluxes in 2-D at reach scale. The 2-D represents longitudinal and vertical section. b) Figure below represents hyporheic zone fluxes at local scale. The effect of pool and riffle sequences are changing the flow patterns. Red and blue arrows indicate water and heat fluxes.

There are various existing methods for measuring the groundwater-surface water interactions, and quantification models (Kalbus et al., 2006; Boano et al., 2014). A method based on Darcy's law with introducing standpipes into the hyporheic zone through vertical column standpipes. This method is advantageous against slug tests, permeameter tests, or grain-size analysis in determination of streambed hydraulic conductivity and anisotropy. However, limitations with similar methods are that the results can vary over orders of magnitude (Chen, 2000) and difficult to determine in-situ (Cardenas and Zlotnik, 2003) for stream tracer tests using dye or other conservative tracers.

The dynamic distributions of thermal conditions present in saturated near-surface sediments have been widely utilized to quantify the flow of water (Anderson, 2005). A rapidly increasing number of papers demonstrate that heat as a tracer is becoming an integral part of the toolbox used to investigate water flow in the environment. The method is based on the fact that the temperature distribution in the subsurface medium is not only the result of heat conduction, but also of advection by moving water through the porous medium (Stonestrom and Constantz, 2003). The stream temperature is

subject to diurnal temperature variation, as well as changes through summer, and winter season. The aquifer temperature is more stable, and its seasonal fluctuations are low. These phenomena cause temperature differences between surface water - ground water which enables us to estimate the heat and water exchanges between the stream and the aquifer. The use of HZ temperature time records to identify losing and gaining points among a river was qualitatively investigated by Silliman and Booth (1993). They conducted that the temperature measurements at different depths provide an excellent indicator for water flow. Constantz (1998) found that the variations in surface water and sediment temperatures are greater for losing reaches than for gaining reaches. Exchange patterns can be inferred quantitatively from HZ temperature time records (Lowry et al., 2007; Schmidt et al., 2007; Stonestrom and Constantz, 2003).

Temperature can be measured easily and rapidly, especially since cheap, robust sensors, and data loggers have become readily available (Cucchi et al., 2018). Temperature surveys alone are not sufficient to accurately interpret the magnitude of water fluxes. A novel study by Cucchi et al. (2018), proposes a method which fully couples pressure differential time series with temperature time series recorded from the hyporheic column.

A limitation for this method was that the loggers were bound to the local scale until recently. A new technology is put into use recently which overcomes these problems. Selker et al. (2006a) introduced fiber optics distributed temperature sensing (FO-DTS) to sense the interaction of groundwater and surface water along a river channel from temperature signals. This method is deployed to evaluate the temperature dynamics at the sediment-water interface with an emphasis on the biological life by Rosenberry et al. (2016), to estimate the groundwater inflow zones as well as hyporheic inflow zones in arid climatic areas (Yao et al., 2015), and to quantify the surface water - ground water interactions by coupling the FO-DTS with vertical hydraulic gradients estimated by point in space stations (Huang et al., 2016). Hence, there is an opportunity to use this method for variety of applications to estimate, and quantify the biological, ecological, and physical characteristics of surface water - ground water exchanges in the river channel.

1.2 Statement of the Problem

This thesis focuses on the investigation of the spatial and temporal variability of water and heat fluxes along a stream channel with emphasis on the effects of the pool and riffle sequences. The specific objectives of this study were to (i) evaluate the use of FO-DTS for mapping the up-welling and down-welling zones (pool and riffle effects) along a 1 km reach, (ii) estimate the hydro-thermal parameters and the 1-D water vertical fluxes from the data recorded by the mini-LOMOS with an inversion script and a hydro-thermal model, and (iii) integrate DTS temperature observations with mini-LOMOS data to determine the spatio-temporal variation of the water and heat fluxes along the reach. For the last goal, a 2-D hydro-thermal transect model was constructed by prescribing the FO-DTS temperature at the surface and the hydro-thermal parameters obtained using the mini-LOMOS. With these objectives, we aim to seek answers to "is it possible to use the hydro-thermal parameters estimated with a 1-D model in a 2-D model at reach scale". This question is important since the hydro-thermal parameters estimated in 1-D vertical profiles represents local scales, however, at local scale, the spatial heterogeneity might affect the estimated parameters since they are local and would not represent the whole studied medium. The second question is "are we able to represent the effects of pool and riffle sequences without data set".

2. METHODS

2.1 Heat as a Tracer for Stream-Aquifer Interactions

Heat is a naturally occurring and transporting phenomena. As it is naturally occurring, it is cheaper to monitor with specific gadgets and use it as a tracer (Anderson, 2005). Heat is used as a tracer to understand the river-aquifer interactions for at least a decade with growing attention (Constantz, 1998; Constantz, 2008). The use of heat has a tracer to quantify surface water-ground water (SW-GW) exchange has become well established based on the pioneering work by Suzuki (1960), Stallman (1965), and Bredehoeft and Papaopulos (1965). The river temperature variation by day is between 1°C and 10°C as a function of season and the seasonal variation can reach to 30°C. The yearly variations of the aquifer temperature are generally less than 1°C. Methods based on diurnal temperature signals (e.g. Hatch et al., 2006, Keery et al., 2007) have become increasingly popular, because they yield vertical fluid flux estimates in time for both up-welling and down-welling cases, with minimal effort, small experimental footprint, and relatively low cost. The widespread use of diurnal temperature signal methods has been facilitated by pressure difference and temperature sensor (Cucchi et al., 2018), in signal processing methods (Onderka et al., 2013), and the availability of automated software to process temperature data (Munz et al., 2016). The basic theory of the use of heat as a tracer is the heat transport equation (Eqn. 2.1) (de Marsily, 1986):

$$\Delta(\lambda \Delta T - \rho_w C_w U T) = \rho C \frac{\delta T}{\delta t} \qquad (2.1)$$

λ: the equivalent conductivity tensor between the solid medium and the water ($Wm^{-1}K^{-1}$),

T: the temperature (K),

$\rho_w C_w$: the density and specific heat capacity of water ($Jm^{-3}K^{-3}$),

$\rho_s C_s$: the density and specific heat capacity of solid ($Jm^{-3}K^{-3}$),

ρC: the specific gravity and specific heat capacity of porous medium (water + solid) ($Jm^{-3}K^{-3}$) ($C = (1-\omega)\rho_s C_s + \rho_w C_w \omega$),

ω= total porosity,

U = Darcy velocity (ms^{-1}),

This equation represents two physical processes: (a) The transport of heat by conduction as well as transport by thermal dispersion (analogous to hydrodynamic dispersion in solute transport theory). It includes effects of conduction through the rock-fluid matrix as well as the effects of thermal dispersion, which is caused by velocity variation within the pore space. (b) The transport of heat by flowing water, a process known as advection (Constantz, 1998).

The Figure 2.1 summarizes the qualitative relationship between water and sediment temperatures for gaining and losing stream conditions. Temperature profiles beneath streams are elongated in losing reaches where stream water recharges the aquifer and compressed in gaining reaches (Figure 2.1.a). For the case of gaining stream (Figure 2.1.b), the hydraulic gradient is upward (higher head in the HZ than in the stream) as indicated by the higher altitude of water in the piezometer than in the stream stage. The stream has a large diurnal variation in water temperature. The HZ has only a slight diurnal variation because water is flowing up from aquifer where temperatures are constant on diurnal time scales. Variation in HZ temperature HZ reflects the balance between the oscillating transport of heat via conduction and upward transport of heat via advection. At any given depth beneath the HZ, higher flows of groundwater to the stream lead to smaller variations in HZ temperature while smaller flows lead to larger temperature variations. For the case of a losing stream (Figure 2.1.b), the hydraulic gradient is downward (lower head of HZ than in the stream). The downward flow of water transports heat from the stream into the sediments. The downward advection of heat results in larger diurnal fluctuations in HZ temperature. In addition, since regional groundwater is not flowing into the stream, temperatures vary more in losing streams than in gaining streams (Constantz, 1998).

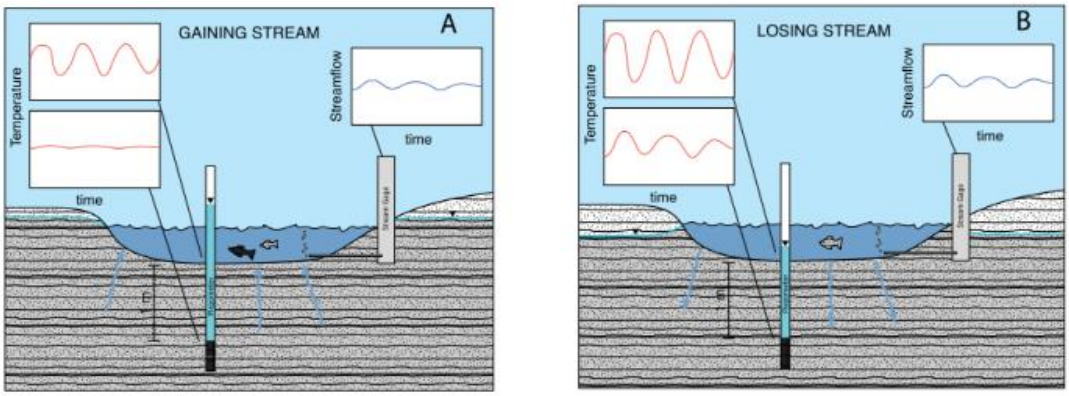

Figure 2.1: Hydraulic and thermal responses in streambeds under influence of streamflow for (a) gaining stream, (b) losing stream. The figure is modified from Constantz (2008).

The seasonal temperature variation in hyporheic column is illustrated at Figure 2.2. In Winter, the aquifer is warmer than river, and in Summer, the river is warmer than the aquifer. In the case of gaining stream, the temperature difference occurs in much lower depth, unlike the losing stream, where the stream can propagate deeper parts in the hyporheic zone and affect the temperature variation.

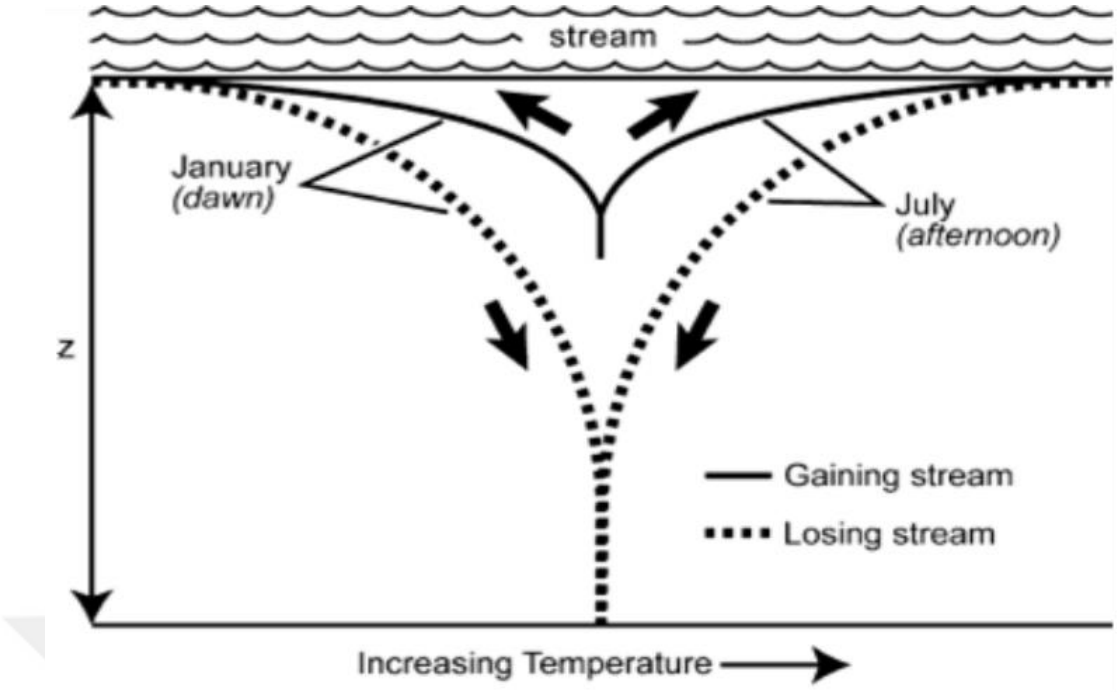

Figure 2.2: Seasonal temperature variation in hyporheic zone as a function of depth. The figure is taken from Anderson (2005).

2.2 Description of the Study Site: Avenelles Basin

Avenelles basin is a part of Orgeval catchment. The catchment is a part of Seine basin situated in north of France. Avenelles basin is at 70 km east of Paris. The study site comprises a 1.1 km portion of Avenelles river.

2.2.1 Study site

Avenelles river is well instrumented and recorded for over 30 years, by various institutions, and it's a part of the research activities of PIREN-Seine (PIREN-Seine, 2018). The catchment is formed on 104 km^2 area for Orgeval. Avenelles basin covers 46 km^2 inside Orgeval basin. Agriculture covers 80% while the remaining area is forested. Average annual air temperature is 11°C. Annual mean precipitation is 658 mm over the period of 1963-2010 (with a standard deviation of 111 mm)(Mouhri et al., 2013), and annual mean potential evaporation is 592 mm. The basin represents low relief: the altitude varies between 130 m to 187 m above sea level for the 80% of the

area. The hydrometeorological conditions in the study site for the studied year are shown in Figure 2.3. The peak precipitation is 24.3 mm at June, whereas the mean monthly precipitation is 34.6 mm. The average air temperature during the year is 10.0°C, with T_{min}=-4°C, and T_{max}=38.5°C. The average discharge is 157.6 L/s where Q_{max}=1780 L/s.

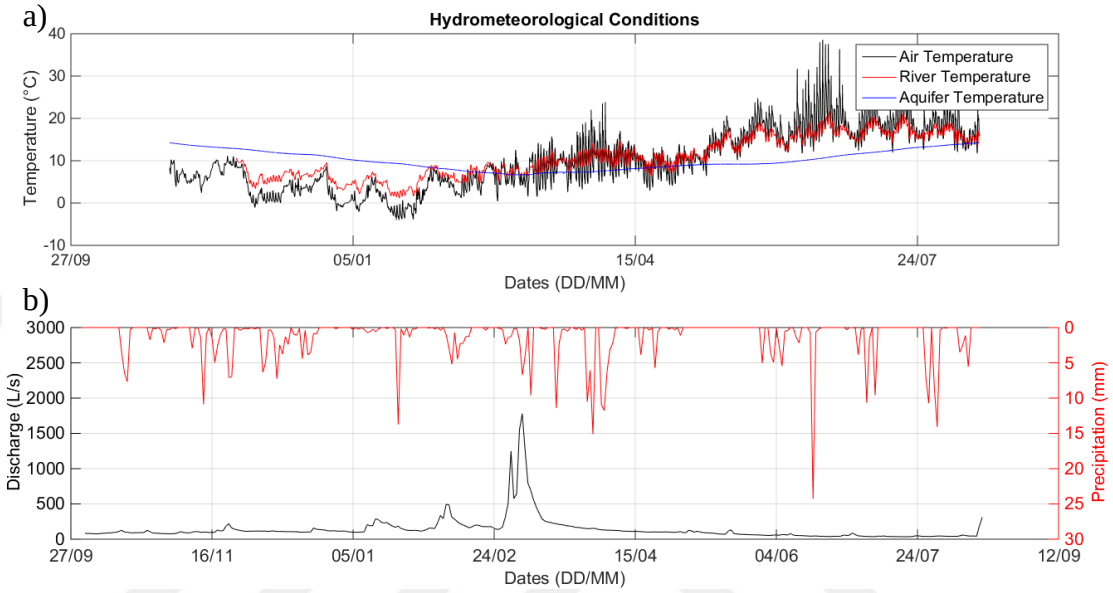

Figure 2.3: Hydrometeorological conditions at the study area from BDOH (Tallec et al., 2015). a) This figure represents air temperatures, river, and aquifer temperatures from Bertin station. b) This figure represents precipitation and river discharge. The period of screening is: 1 October 2016 - 1 October 2017.

Two main geological units influence the hydrogeological output of the Orgeval Basin: the Oligocene (i.e. Stampian sand and Rupelian limestone) and the Middle Eocene (i.e. Bartonian limestone). These geological units form the aquifers of the catchment area, whom are divided by a clayey aquitard, namely, Priabonian mudstone and Bartonian marl. The surface is mainly covered with table-land loess with a 2-5 m varying thickness. The aquifers and the stations of LOMOS are shown in Figure 2.4.

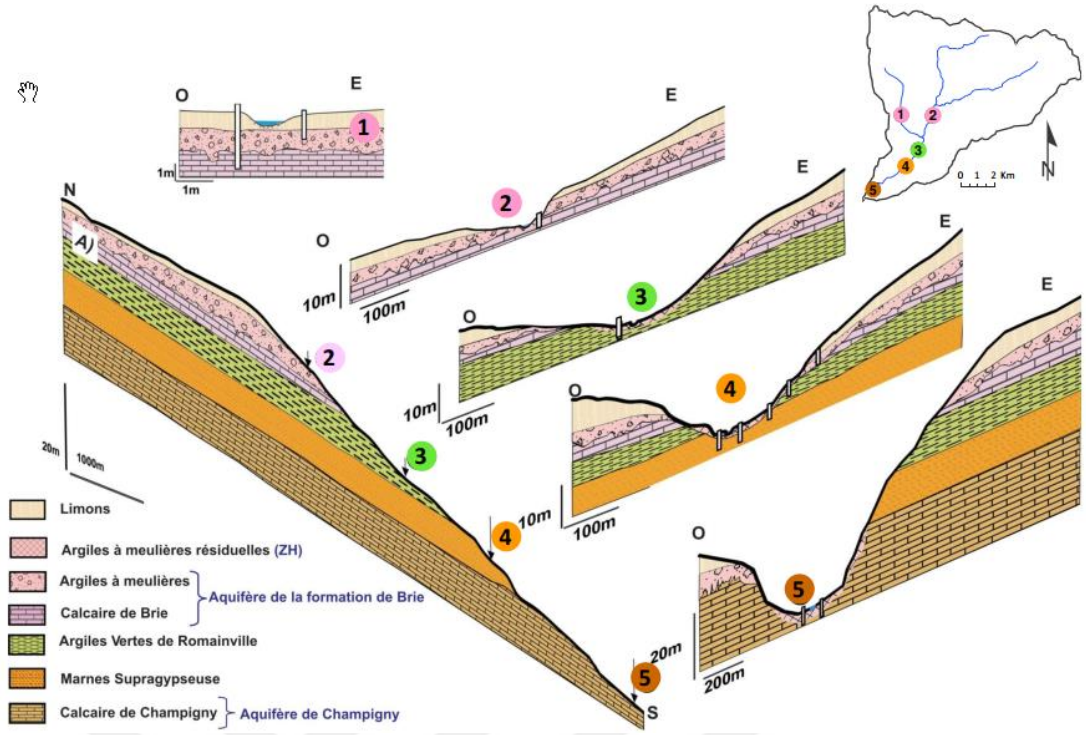

Figure 2.4: The lithological profiles of LOMOS stations with their distributions in Orgeval basin.

Surface water-groundwater interaction was actively investigated in the area (Berrhouma, 2016; Mouhri et al., 2013; Flipo, 2013). Mouhri et al. (2013), have deployed stream-aquifer exchanges monitoring system on the basin, based on 5 LOcal MOnitoring Stations (LOMOS) distributed along 6 km Avenelles river network.

Each LOMOS is composed of one or two shallow piezometers located 2 to 3 m away from the river edge; one surface water monitoring system, two hyporheic zone temperature profiles located close to each river bank. The five LOMOSes are distributed in two upstream, two intermediate, and one downstream position. At each LOMOS, water pressure and temperatures have been monitored with a 15 minutes time step for 5 years. This data set is interpreted by the usage of the method of the heat as a water flow tracer to analyze the variability of the interface hydrological functioning using heat as a flow tracer (Berrhouma, 2016).

A FO-DTS unit has been set up since October 2016 along 1.1 km river to improve the description of water and heat fluxes between the stream and the aquifers.

2.2.2 Study site: reach scale

The fiber optic cable was laid between the Bertin LOMOS and the Petit Paris LOMOS situated at the center part of the basin (Figure 2.7). Starting point of the FO-DTS survey (the 0th m) is Bertin station. The cable is laid on upstream portion of the Avenelles River. According to Berrhouma (2016), the river is connected to the Brie aquifer unit. This LOMOS is characterized by an alternation of infiltration and exfiltration periods. During the low flow, the mean discharge is 53 L/s, contrary to, 143.5 L/s flow during high flow.

This station is characterized by a large colluvium plain and the two aquitard layer (green clay and marn, see Figure 2.5, Figure 2.6). Along the river corridor, there are three distinct concrete slabs in the river: one long slab at the downstream part of the confluence, and two concrete slabs beneath both bridges.

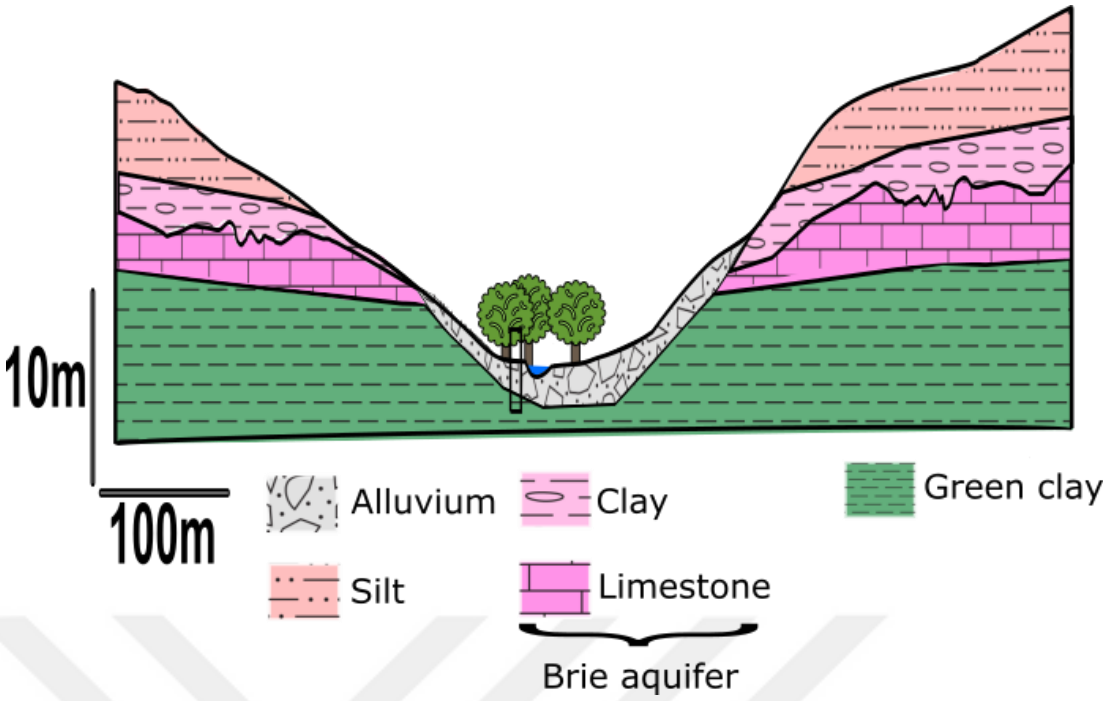

Figure 2.5: Lithological profile of Bertin station, the area is predominantly colluviums.

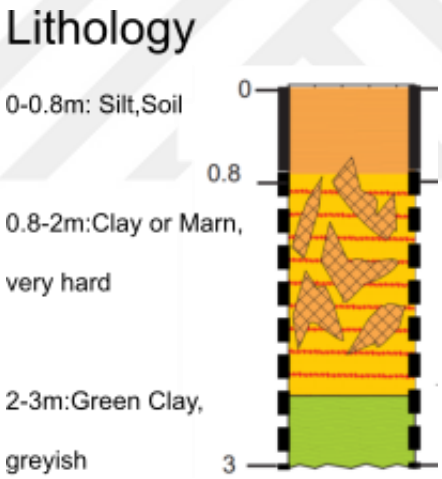

Figure 2.6: The columnar section of Bertin station from previous studies (659434.3 E,2427873.85 N).

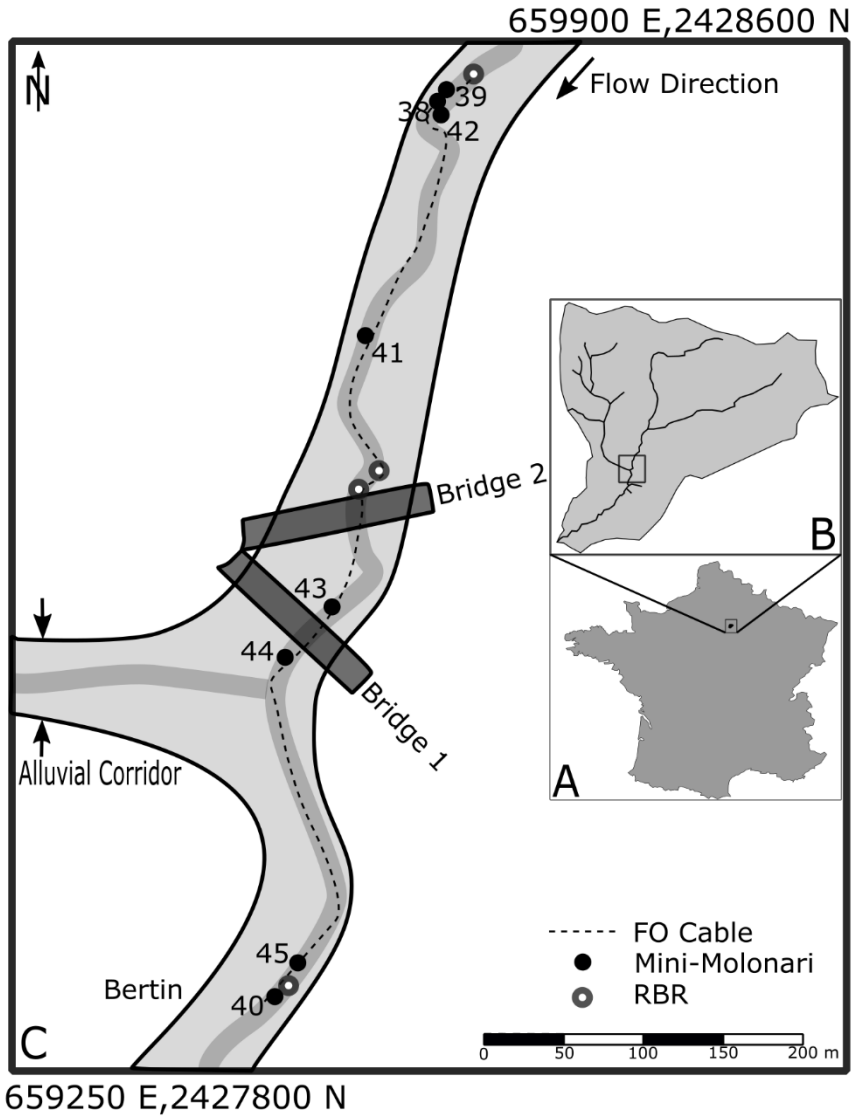

Figure 2.7: FO-DTS Setup in the Avenelles river. The survey starts from Bertin, where the instrument is located and set upstream. Three high resolution RBR probes were deployed to compare measurements of FO as well as 8 mini-LOMOS stations in various locations throughout the river within different time intervals. The figure is developed in the geological map provided of the area. The coordinates mark the northeast and southwest corners of the map

2.2.3 Topography survey

A topography survey is completed during a field excursion between 14-18 April 2018. The purpose of this survey was to measure the characteristics (position along the FO-DTS cable, altitude, river water level) the pool and riffle sequences in the study area.

The survey was carried on by a tripod, a manual level, and a measurement pole. The goal is to take measurement at the beginning, in the middle, at the end of each pool, and riffle. The result of topography survey is given in Figure 2.8. In each measurement, the station as referenced with a FO-DTS cable meter. A total of 196 stations were measured. The collected data was validated with an IGN satellite digital elevation model (DEM) with a 5 m resolution. Both profiles had the same slope, however, the satellite DEM was 2 m lower than the surveyed topography profile as can be seen in Figure 2.9. This is due to the resolution difference between DEM and the measured data.

The physical references such as concrete cascades, confluence, bridges were collected. The altitude of the studied section is ranging between 112.7 m to 121.3 m over a 1063 m longitudinal path. The end of the topography is at 1063 m where the FO-DTS cable ends.

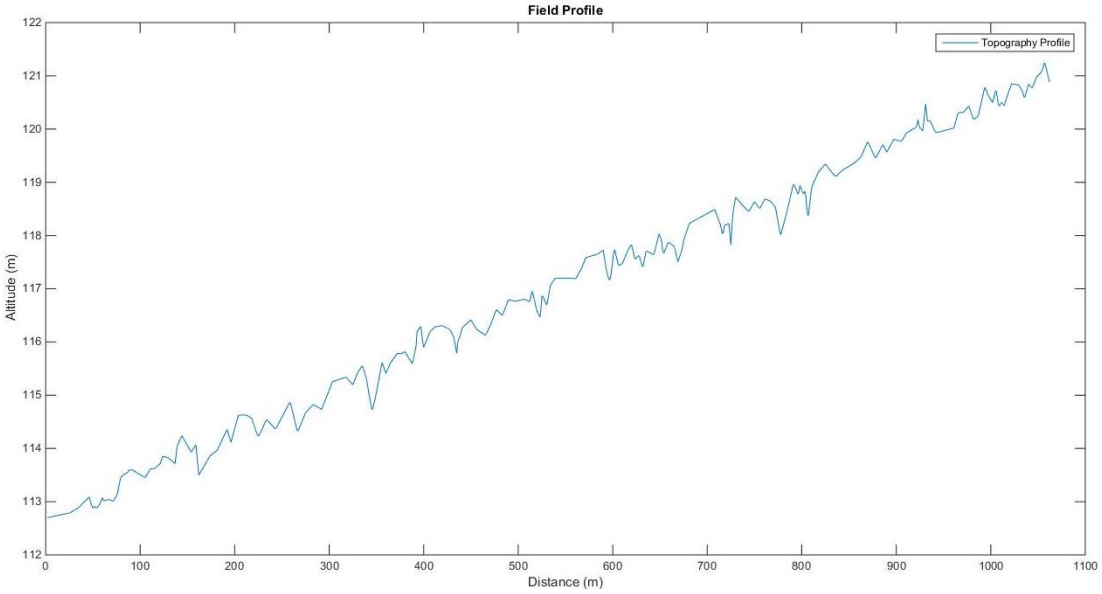

Figure 2.8: Topography section of the Avenelles River. The figure represents 196 measured points. The collected data is later enriched and smoothed on MATLAB platform (MathWorks, 2018).

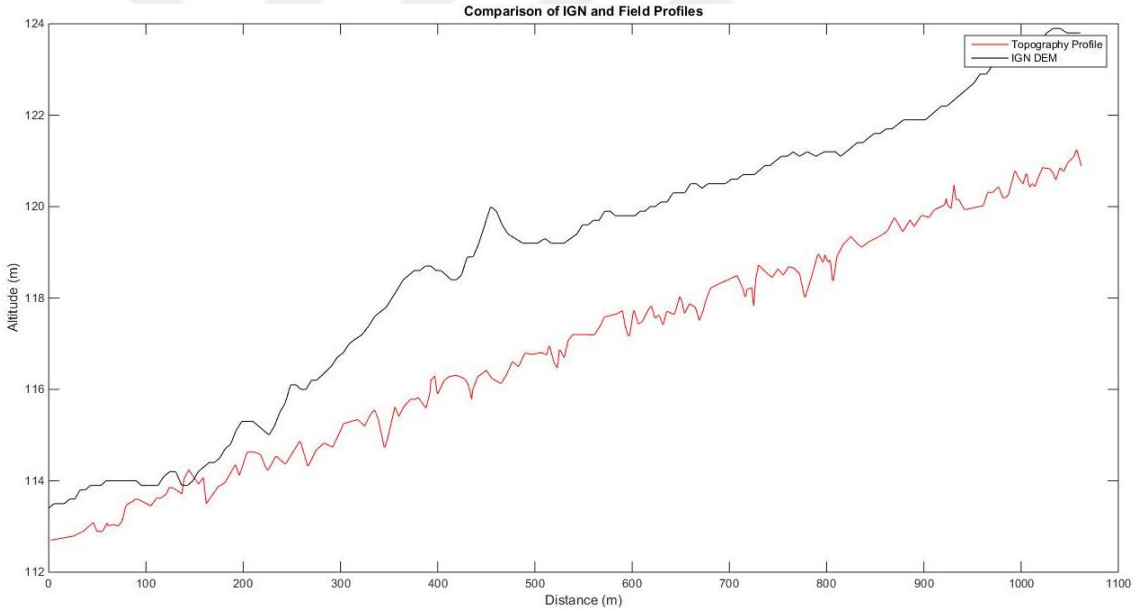

Figure 2.9: The validation of topography survey by IGN satellite DEM. The altitude difference is due to the resolution of DEM, which is 5 m. Therefore, the DEM covers a wide area for the riverbed and naturally, it represents the average altitude of the area.

2.3 Experimental Setup

Field data was recorded from four instruments: FO-DTS, Mini-LOMOS, LOMOS, and temperature sensors (RBR). The Figure 2.10 synthesizes the position of each instrument and their recorded periods

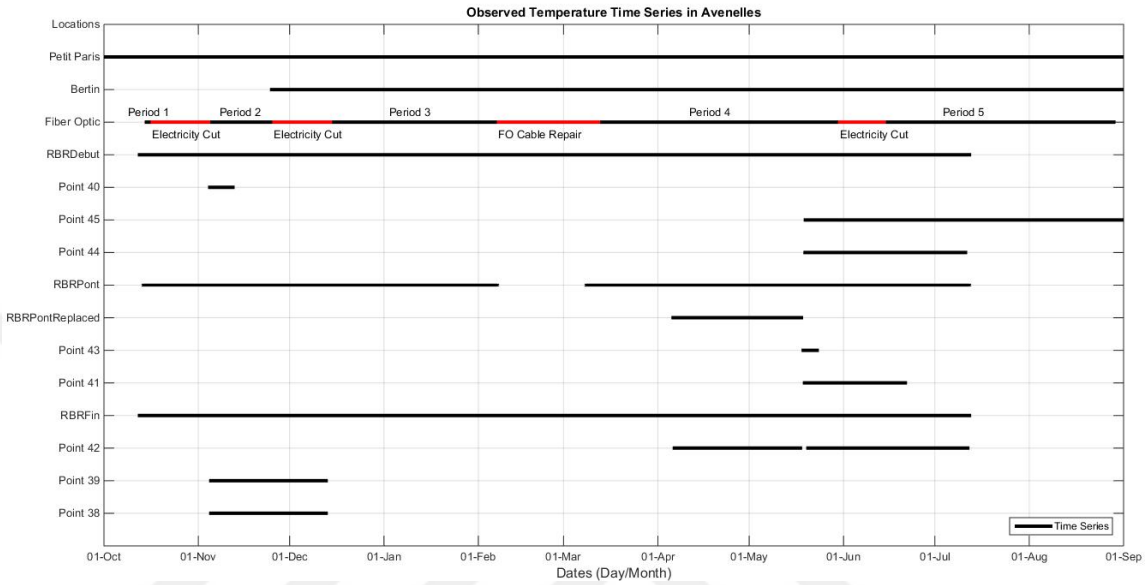

Figure 2.10: Data collected during the survey period. FO-DTS survey has stopped during 4 periods (red lines). These stops were due to electricity cut, and a stop for repair.

2.3.1 FO-DTS unit

Principles and functioning

The FO-DTS technology has found its ground in a wide range of applications in environmental monitoring recently as a crucial tool for measuring temperature with high spatial, and temporal resolution (Selker et al., 2006b; Selker et al., 2006a). The FO-DTS method (see Figure 2.11) became a strong tool for hydrologists in various ways: active distributed temperature sensing applications for quantifying flow in boreholes (Read et al., 2014) or thermal plume fiber optic tracking tests for groundwater velocity measurements (Read et al., 2015), or estimating seepage rates by obtaining vertical temperature profiles (Vogt et al., 2010), and for estimation of bedload transport under flood conditions (Bray and Dunne, 2017). The tool proved to be an alternative to the other conventional monitoring tools which has limited spatial applications. For instance, Briggs et al. (2012) compared three widely used techniques namely: differential gauging, dilution gauging, and geochemical mixing. They found that FO-DTS provided the finest spatial characterization of stream-aquifer exchanges. In this study, the tool is used to passively monitor the hyporheic zone exchanges at the riverbed, at hyporheic zone interface.

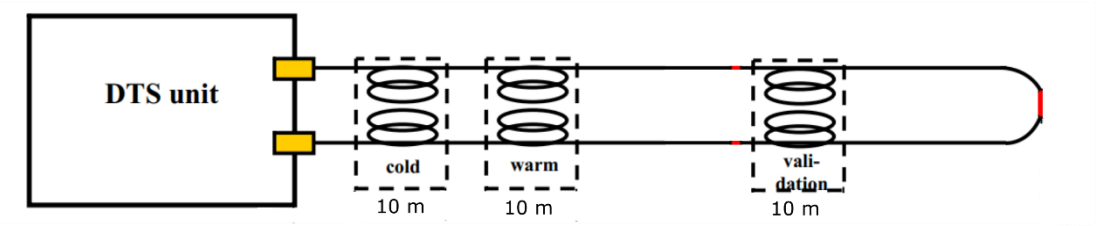

Figure 2.11: Schematic setup of DTS double-ended configuration. Lengths are not to scale. The forward and reverse fibers are enclosed in the fiber-optic cable. The red dots indicate the entrance to water, end of the cable, and exit from the water. Cold and warm baths are next to the FO-DTS unit. The validation probes are buried in the riverbed with a 10 m loop of FO-DTS. Figure is modified from van de Giesen et al. (2012).

The Raman spectra distributed temperature sensing tool measures temperature by sending a laser pulse down the length of the fiber optic cable. Variations in temperature cause differences in backscatter, changing the wavelength and intensity of the light. The scattered light travels back up the fiber as a higher wavelength i.e. Stokes, and lower wavelength i.e. anti-Stokes. The temperature does not affect Stokes, but only the

anti-Stokes. The ratio of the two intensities can be used to calculate the temperatures at different sections of the cable (Lowry et al., 2007).

There are three methods to use FO-DTS:

1) The single ended configuration which consists of a DTS measuring temperatures along the cable with only one connection to the measurement instrument. Single-ended field deployments with non-uniform losses cannot be easily addressed without additional information (Hausner et al., 2011).

2) The duplexed single-ended configuration which consists of two co-located fibers laid on the same path measure the temperature where one is going away from the instrument and the other is coming back towards the instrument (Hausner et al., 2011).

3) The double-ended configuration consists of the two cables taking measurements from both directions and they are connected to the measurement unit (Hausner et al., 2011). This configuration offers an opportunity to refine the data, minimizing the impact of multiple step losses on measured temperatures (van de Giesen et al., 2012).

The choice of method depends on the desired temperature resolution, availability of suitable independent observations to use as reference temperatures, and the experimental design of the study.

Installation

Fiber optic distributed temperature sensing (FO-DTS) unit was installed at the beginning of October 2016. In most of the FO-DTS studies, the cable has been deployed at the surface of the streambed, or vertically towards HZ, resulting in measurements of river temperature or measuring the vertical HZ temperatures. In contrast, in this study, the cable was installed at an average depth of 5 cm within the streambed to directly measure the temperature of the top of the HZ. A total of 1282 m of cable was installed from downstream to upstream of Avenelles river at the top interface of hyporheic zone. Whole portion of the FO-DTS cable was beneath the riverbed buried under rocks, and alluvium. The cable was stabilized with the help of approximately 100 tent pegs and covered with colluvium (Figure 2.12) by hand.

The FO-DTS unit collected temperature measurements each 15 minute with 0.25 cm spatial intervals. The tool was calibrated by a team from University of Rennes, and it was set as double-ended configuration. There were 3 highly accurate RBR temperature probes installed at different portions of FO-DTS cable for data validation purposes. The tool was planned to run from beginning of October 2016 to end of July 2017. During the installation, there were eight loops of 10 m each to increase the spatial resolution in the selected pools as one of the goals is to observe the behavior of the riffle-pool system.

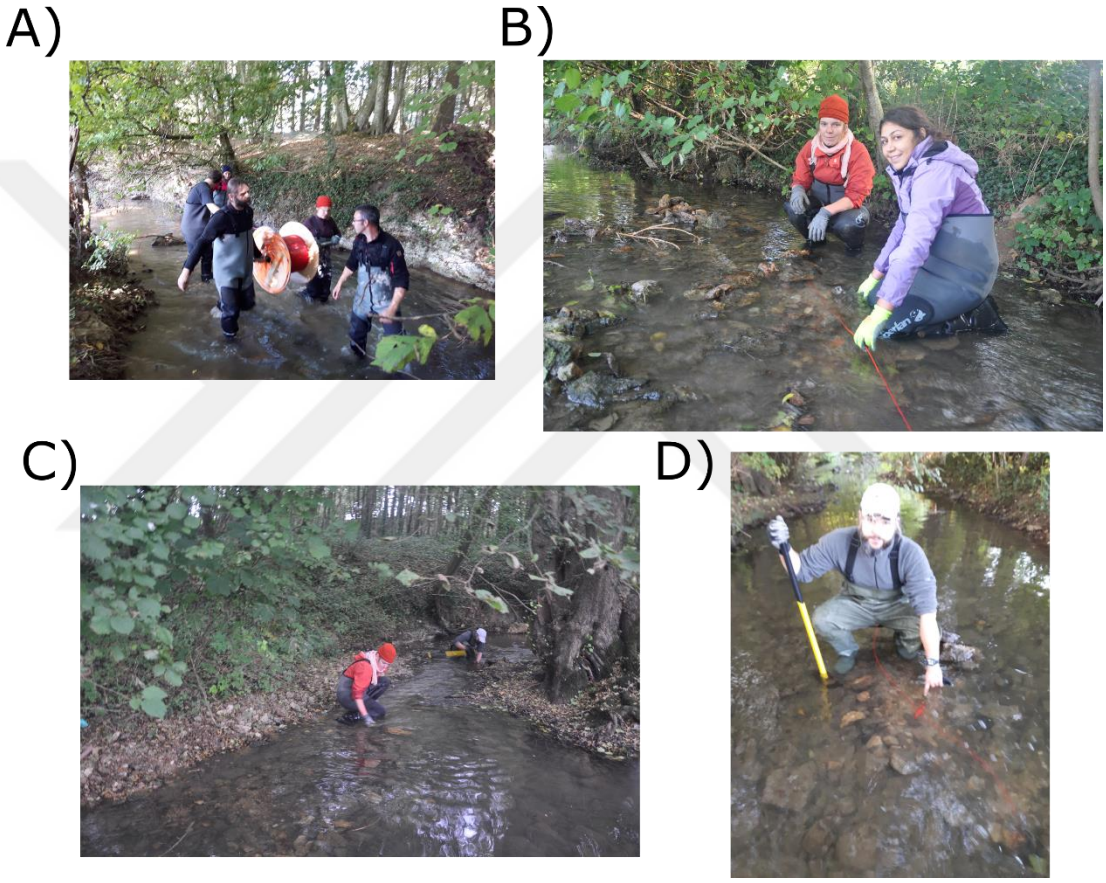

Figure 2.12: A) Installation of the FO-DTS, B) covering under the colluvium, C) installation at riverbed, and D) securing and hiding with tent pegs.

Calibration

In this study, the tool was calibrated by a team from University of Rennes, and the FO-DTS unit was set in double-ended configuration. There is also in-situ calibration with a hot and cold bath, with known temperatures. These baths are helping the tool to

reference the measured temperatures throughout the cable and as a result, the tool provides finer resolution (Tyler et al., 2009).

During the monitoring period, hot bath failed after an electrical failure, then a portion of the cable spliced and repaired. The temperature measurements varied up to 2.5°C from the RBR data logger results. Therefore, the collected data was re-calibrated from double-ended configuration to single-ended configuration to increase the accuracy of the measured temperatures.

Validation

The validation of FO-DTS temperature data was done by comparing the temperature with 3 highly accurate RBR temperature probes. The RBR temperature probes were installed at the beginning of FO-DTS cable (Bertin station, in the river), at the second bridge (610 m), and at the end of the FO-DTS cable (at 1083 m). Each of these probes was attached to FO-DTS cable. A loop of 10 m long FO-DTS cable was circulated around the probes to increase the accuracy of FO-DTS temperature profiles. Moreover, during the installation, there were eight loops of 10 m installed at selected pools to improve the monitoring accuracy.

2.3.2 Mini-LOMOS

Mini-LOMOS is a novel tool for obtaining temperature and hydraulic head measurements in 1-D vertical column of hyporheic zone. The sensor records the hydraulic difference between the HZ and the river, and the temperature profile (See Figure 2.13). Coupling this sensor with a hydro-thermal numerical code enables us to estimate the hydro-thermal parameters of the HZ and 1-D vertical water and heat fluxes at local scale (Cucchi et al., 2018).

Functioning

The method of deployment, calibration of the sensors, and the principles of the tool are introduced by Cucchi et al. (2018). Mini-LOMOS consists of 2 systems. First system is temperature system, formed by four temperature data loggers installed at different depths which measure the temperature profile of the HZ and one temperature

sensor located in the river. The second system is pressure differential system where it measures the difference between hyporheic zone pressure and riverbed pressure. The temperature and pressure differential time series are monitored constantly with 15 minutes intervals.

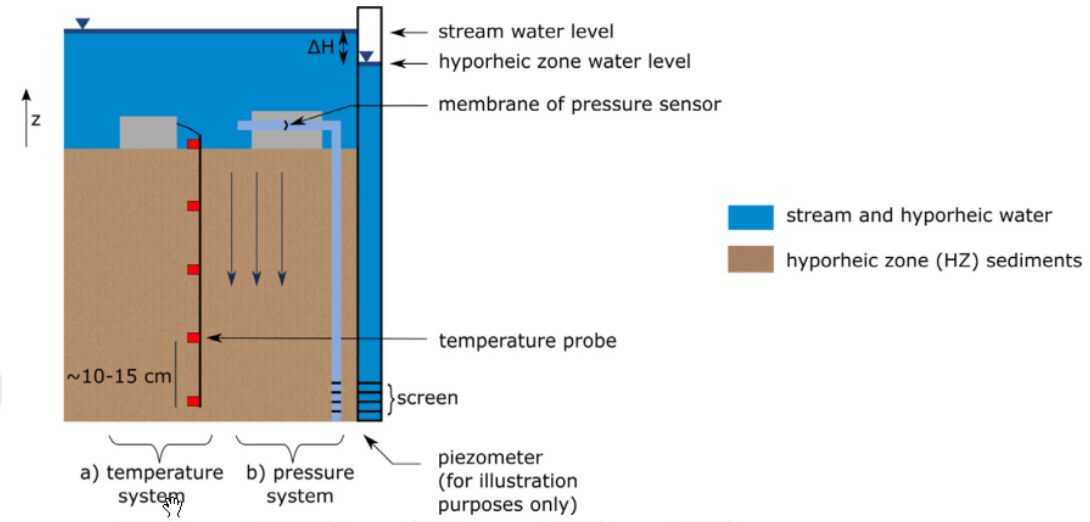

Figure 2.13: Positioning of Mini-LOMOS sensors in the hyporheic zone column. The tool couples (a) vertically distributed temperature time series measurements, (b) hydraulic head differential between the steam and the underlying hyporheic zone. The piezometer next to the pressure system is for demonstration purposes only, not present in the actual setup. The figure is taken from Cucchi et al. (2018)

Field Setup

Mini-LOMOS had been installed in various time periods throughout the hydrological year along the FO-DTS (Figure 2.10). There are three mini-LOMOS installed in Autumn, five installed in Spring and Summer. The position and characteristics of the mini-LOMOS are given in Table 1, Table 2**Error! Reference source not found.**. During the recorded period, some issues have been witnessed:

- P38 : Temperature recorded at riverbed is lower than HZ recordings constantly at least 2°C.
- P39 : Temperature sensors are not working, thus it can not be used for inversions.
- P43 : Battery died after 5 days, temperature sensor at 7 cm does not work.
- P45 : Pressure difference was an order of magnitude higher than other stations.

– Four mini-LOMOS (P40, P41, P42, and P45) have problems with one of their temperature sensors. Therefore, we consider only 3 HZ temperature sensors for the inversion, excluding the ones with problem, for these stations.

Table 1: Mini-LOMOS sensor locations and 1-D vertical depths. The final depth represents the total penetration into HZ at that location by mini-LOMOS. The position starts from Bertin station (0 m)

Name	Position (m)	Sensor 1 (cm)	Sensor 2 (cm)	Sensor 3 (cm)	Sensor 4 (cm)
P38	1034	10	25	40	55
P39	1034	10	25	40	55
P40	4	10	20	30	40
P41	774	10	20	30	40
P42	994	10	20	30	40
P43	436	7	17	27	37
P44	364	8	18	28	38
P45	74	10	20	30	40

Table 2: Working sensors(x) and failed sensors (-). The periods are in format of DD/MM/YY. The value n represents total number of time steps for each station. Each step is 15 minutes.

Name	Temperature	Pressure	Temperature Sensor 1	Temperature Sensor 2	Temperature Sensor 3	Temperature Sensor 4	Period	N
P38	X	x	x	x	x	x	04/11/16-13/12/16	3750
P39	-	x	x	x	x	x	04/11/16-	-
P40	X	x	x	x	x	x	13/12/16 04/11/16-	2526
P41	X	x	x	x	x	x	30/11/16 18/05/17-	3296
P42	X	x	x	x	x	x	21/06/17 05/04/17-	9234
P43	X	x	-	x	x	x	12/07/17 18/05/17-	450
							23/05/17	

Table 2. (cont.)

P44	X	x	x	x	x	x	18/05/17-11/07/17	5177
P45	X	x	x	x	-	x	18/05/17-07/11/17	16576

Estimation of hydrothermal parameters

A thermo-hydrogeological model (Ginette) coupled with a parameters screening script is used to determine the hydrogeological and thermal properties of the HZ (Figure 2.14). Ginette is a fully coupled transient finite volume model solving the water flow and heat transport in porous media (Rivière et al., 2014). The estimated parameters are volumetric heat capacity (ϱC), intrinsic permeability (κ), porosity (ω), thermal conductivity (λ) as in Table 3.

The domain is 1-D column representing the HZ. We use grid discretization 1 cm and an adaptive time series stepping ensuring convergence of numerical simulations. Boundary conditions applied to the domain are the hydraulic head difference time series, as well as the river and HZ bottom temperature time series obtained from the mini-LOMOS device. The initial temperature field cannot be determined from measurements and is unknown. To minimize the influence of initial pressure and temperature fields on inversion results, we introduce a burnout time of 4 days. Hypotheses associated with this methodology are the water and heat fluxes between the stream and aquifer are vertical and homogeneous in the column. The parameters screening script allows us the envisage the horizontal heterogeneities inside the domain.

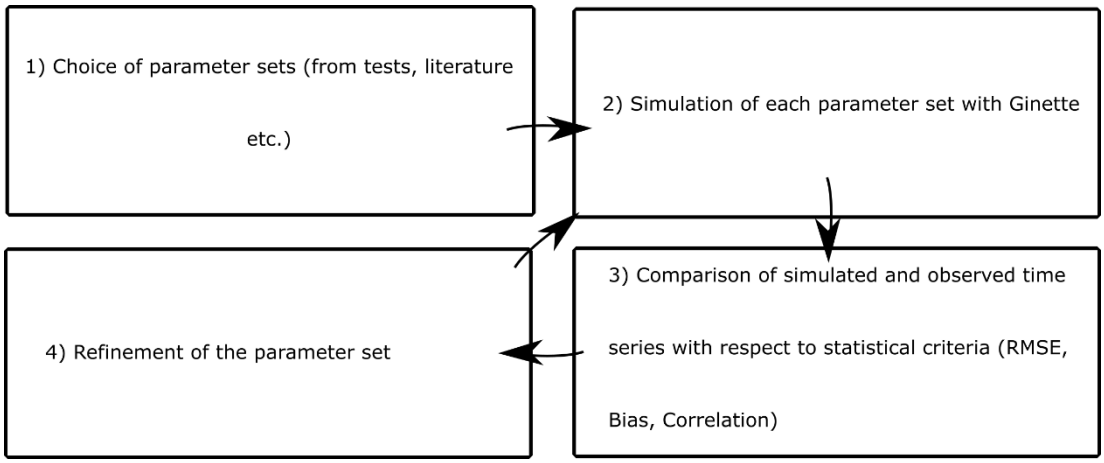

Figure 2.14: Step by step representation of the operating scheme of inversion script using Ginette.

The principle of the inversion script is summarized at Figure 2.14. Initially, the parameter sets are chosen to inverse the temperature and pressure difference time series. Secondly, the simulation is run with given parameter sets. After each run, the parameter sets are compared with respect to statistical criteria as well as simulated time series and observed time series. The final stage is the refinement of the parameter set. This process continues until the parameters are refined within acceptable limits. Table 3 summarizes the parameters used in the inversion. While a few physical parameters are deterministically known, other ones vary depending on geological environments at investigated locations and are therefore considered as stochastic.

Table 3: Physical Parameters used for the inversion script.

Parameter	Notation	Numerical value or range	Unit	Reference
Porosity	N	0.15 - 0.5	-	Fetter (2001)
water density	ϱ_w	10^3	kg m^{-3}	Bejan (2013)
water specific heat capacity	c_w	4185	J $kg^{-1}K^{-1}$	Bejan (2013)
water thermal conductivity	λ_w	0.598	$Wm^{-1}K^{-1}$	Bejan (2013)
sediment density	ϱ_s	1800 - 3000	kg m^{-3}	Eppelbaum, Kutasov, and Pilchin (2014)
sediment specific heat capacity	c_s	800-2500	J $kg^{-1}K^{-1}$	Waples and Waples (2004) ; Eppelbaum et al. (2014)
sediment thermal conductivity	λ_s	1 - 5	kg m s$^{-3}C^{-1}$	Eppelbaum, Kutasov, and Pilchin (2014)
intrinsic permeability	k	10^{-14}–10^{-9}	m^2	Menichino and Hester (2014)
gravitational constant	G	9.81	m s^{-2}	
water dynamic viscosity	w	10^{-3}	kg m$^{-1}s^{-1}$	Bejan (2013)

2.4 2-D Model: Estimation of the Water and Heat Fluxes

A 2-D hydro-thermal transect model was constructed by prescribing the FO-DTS temperature at the surface and the hydrothermal parameters obtained using the mini-LOMOS.

2.4.1 Setup

The 2-D mesh is built to simulate the heat and water fluxes in longitudinal and vertical section of the Avenelles river. The mesh size is determined based on the available data, physical constraints, the topography survey of the riverbed, the geological description of the LOMOS at Bertin and Petit Paris, and the mini-LOMOS positions.

The simulated section is shown in Figure 2.15. The origin of the axes x and z is taken at the left bottom of the domain. The domain is 1 km long. Its thickness varies between 3 m and 11 meters. The grid spacing in the horizontal direction is 0.5 m. The vertical

discretization is 0.5 m for the first 2.5 meters deep and the rest of the domain has a vertical discretization of 0.1 m. The surface of the domain is the topography of the riverbed (presented in section 3.1.1). As a result, there are 98546 cells.

There are 7 zones determined with the help of previous studies of mini-LOMOS inversions, and lithological data. Boundary conditions and zones are summarized in Figure 2.15. The top boundary is the temperature time series recorded by the FO-DTS. The bottom boundary is the temperature recorder in the aquifer piezometer of Bertin. A no-flow boundary is used at the bottom boundary of the domain. The lateral boundaries are "free boundary". That means the numerical code prescribes the temperature calculated at the previous time step. HZ heads do not respect the hydrostatic head principle; "free boundaries" are prescribed beneath the river at the lateral edge of the model. The bottom 2 meter of each side is Dirichlet boundary:

– the head measured in the piezometer of Bertin for the left edge

– the hydraulic head recorded in the piezometer of Petit Paris for the right edge

Imposed hydraulic heads at the surface are calculated from the river water level measured at the both stations and the elevation of geomorphologic discontinuities of the riverbed (cascade). Finally, the model was run for different time periods for each season (21 days for November, 55 days for Winter, 80 days for Spring, 27 days for Summer).

Validation is conducted with mini-LOMOS stations P40, P41, P42, P43, P44, P45. The Spring and Summer season validation is conducted with the stations P40, P41, P42, P43, P44, P45. The Autumn season validation is completed by comparing to station P40.

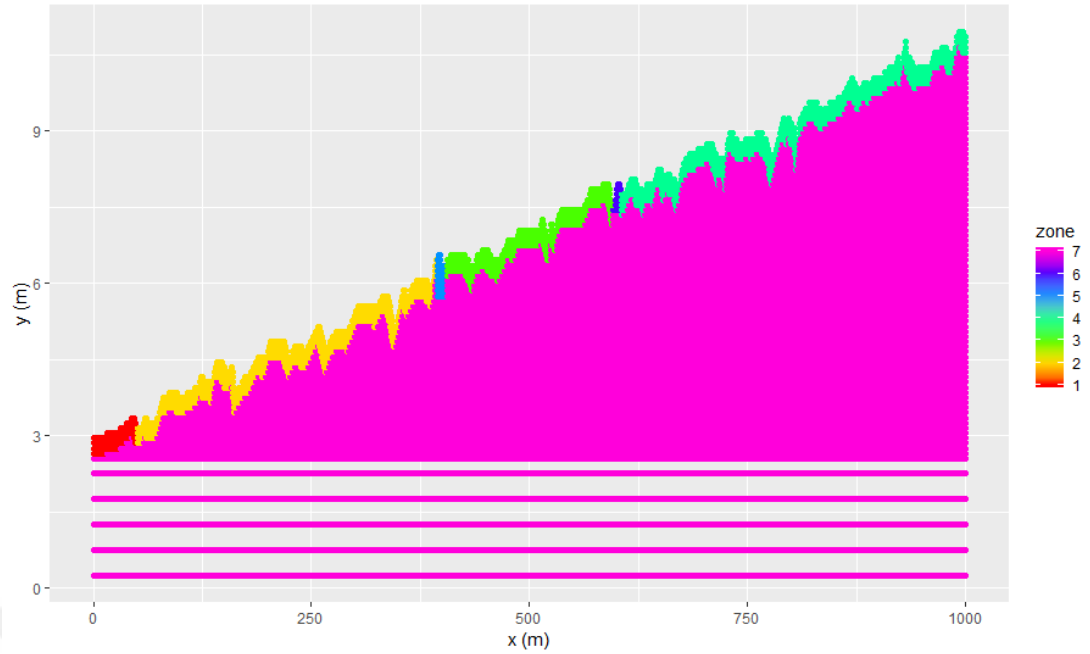

Figure 2.15: Imposed zones on the active cells. Each color represents a distinct zone, which has a unique parameter set obtained from mini-LOMOS. Topography data is from the topography survey. The red lines represent temperature boundary conditions, blue lines are water boundary conditions. Dash line represents no flux, and line for Dirichlet conditions.

The temperature series of mini-LOMOS stations are used to validate the choice of physical and thermal parameters obtained with the 1-D inversion. The parameters imposed on each zone are shown in Table 4.

Table 4: Parameters imposed on each zone

HZ Properties	Unit	Zone 1	Zone 2	Zone 3	Zone 4	Zone 5	Zone 6	Zone 7
Porosity	-	0.35	0.40	0.35	0.25	0.15	0.05	0.15
Intrinsic	m^2	$0.10E^{-12}$	$0.10E^{-11}$	$0.10E^{-12}$	$0.12E^{-12}$	$0.10E^{-11}$	$0.15E^{-13}$	$0.10E^{-13}$
Solid thermal	$kgms^{-3}C^{-1}$	2.0	1.2	2.5	1.8	2.5	2.5	2.8
Solid mass heat	$Jkq^{-1}K^{-1}$	10^4	10^4	10^4	10^4	10^4	10^4	10^4
Specific density	kgm^{-3}	2700	2200	1500	2500	3500	3500	3500

3. RESULTS AND DISCUSSION

3.1 Field Data

In this section, the data from DTS system, Mini-LOMOS, and piezometers will be evaluated.

3.1.1 Characterization of pool and riffle sequences

The geometrical and physical characteristics of pool and riffle sequences are important as they control the discharge, hyporheic exchanges, and biogeochemical conditions (Tonina and Buffington, 2007; Trauth et al., 2014). The pool systems in the Avenelles river are analyzed in Table 5. The basis of the analysis is represented on Figure 3.1. the average depth is 0.29 m. Maximum observed depth in the pool systems is 0.9 m, and the minimum depth is 0.1 m. The main slope over 1063 m is 0.01. The average downstream slope of the pools in the studied section is -0.05. The average upstream slope of the pools in the studied section is 0.05.

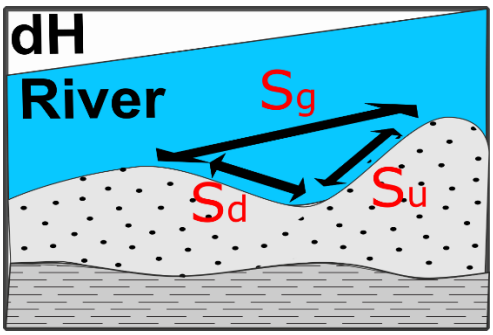

Figure 3.1: The analysis of the pool sequences. Sd signifies the slope downstream, Su is the slope upstream. The Sg is the general slope.

The size of the pool and riffle systems are important. The analysis of the lengths is shown in Figure 3.2. The average length of pool and riffles are around 12 m. There are 3 exceptions for pool, which are longer than 30 m, and 2 exceptions for riffle, which are bigger than 40 m. Dominantly, length of pools range between 10 to 17 m, whereas riffle system has a range of 6 to 15 m.

Table 5: The analyses of the pools in the studied topography section. The downstream slope (Sd) is the slope closer to downstream from the deepest point of the pool. The upstream slope (Su) is the slope of upstream section starting from the bottom of the pool. General slope (Sg) is the slope between beginning and end of the pool.

Class	Class	Length	Depth	Downstream slope of	Upstream slope of	General slope
Pool	1	14	0.2	-0.02	0.04	0.00
Pool	2	10	0.1	-0.01	0.06	0.02
Pool	3	22	0.1	-0.01	0.01	0.00
Pool	4	14	0.2	-0.02	0.07	0.01
Pool	5	10	0.2	-0.02	0.02	-0.01
Pool	6	23	0.6	-0.20	0.03	0.01
Pool	7	11	0.3	-0.08	0.06	0.02
Pool	8	12	0.4	-0.05	0.03	0.02
Pool	9	14	0.1	-0.01	0.03	0.02
Pool	10	15	0.6	-0.07	0.03	0.01
Pool	11	14	0.1	-0.01	0.04	0.02
Pool	12	12	0.9	-0.08	0.09	0.00
Pool	13	15	0.2	-0.05	0.03	0.01
Pool	14	12	0.2	-0.03	0.12	0.03
Pool	15	11	0.4	-0.13	0.04	-0.01
Pool	16	7	0.4	-0.07	0.08	0.01
Pool	17	15	0.3	-0.02	0.04	0.01
Pool	18	19	0.1	-0.02	0.04	0.02
Pool	19	10	0.2	0.00	0.07	0.02
Pool	20	9	0.5	-0.06	0.20	-0.01
Pool	21	17	0.2	-0.04	0.05	0.02
Pool	22	17	0.5	-0.08	0.00	-0.04
Pool	23	8	0.3	-0.06	0.03	0.01
Pool	24	11	0.2	-0.05	0.00	-0.03
Pool	25	24	0.2	-0.03	0.07	0.01
Pool	26	6	0.1	-0.01	0.07	0.02
Pool	27	14	0.3	-0.06	0.04	-0.01
Pool	28	8	0.3	-0.07	0.06	0.03
Pool	29	5	0.5	-0.06	0.10	-0.03
Pool	30	11	0.4	-0.20	0.18	0.07
Pool	31	8	0.2	-0.01	0.02	-0.01
Pool	32	18	0.1	-0.02	0.04	0.01
Pool	33	20	0.4	-0.08	0.06	0.03
Pool	34	32	0.4	-0.10	0.12	0.02
Pool	35	11	0.2	-0.02	0.02	0.01
Pool	36	8	0.3	-0.04	0.03	-0.01
Pool	37	9	0.1	-0.03	0.03	0.01
Pool	38	7	0.1	-0.01	0.04	0.01
Pool	39	30	0.6	-0.05	0.02	-0.01
Pool	40	11	0.2	-0.04	0.05	0.02
Pool	41	7	0.3	-0.04	0.07	-0.01
Pool	42	12	0.3	-0.07	0.03	0.01
Pool	43	17	0.2	-0.04	0.05	0.00
Pool	44	3	0.3	0.00	0.03	0.02

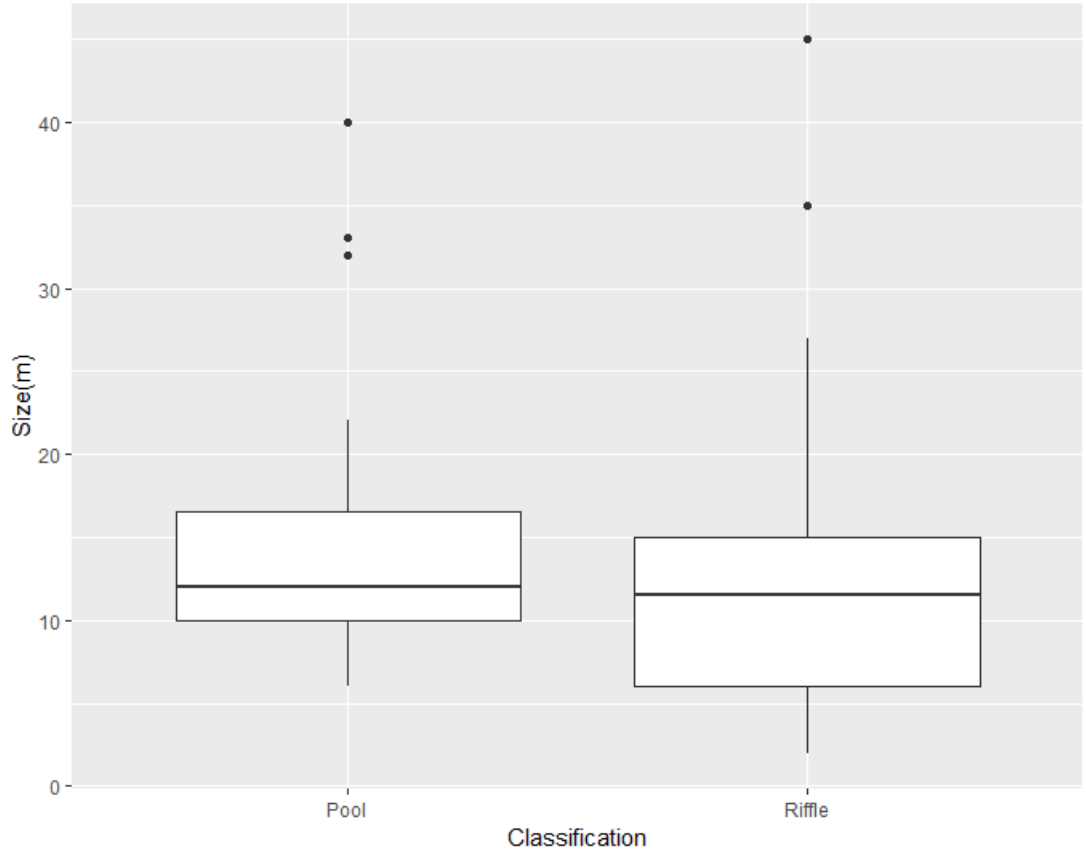

Figure 3.2: The size variation of pool and riffle sequences.

3.1.2 Temperature data from DTS systems

Validation of the data

The difference of FO-DTS data and the validation RBR probes are shown in Figure 3.3. Validation of the data is completed in two periods. Until February, the temperature difference in each validation position is less than 0.01°C. The temperatures of RBR is in good correlation with the temperatures in the FO-DTS.

After March, the difference between FO-DTS cable and RBR probe was as high as 2°C for latter 3 periods (Figure 3.3). This trouble is related to a splice occurred at 797 m. Then, a single-ended method was used to improve the calibration for this period. The temperature differences in each section reduced to 0.5°C. However, the temperature differences at the diurnal temperature peaks are still high. This can be explained by the fact of the hot bath was not operating during these 3 periods and FO-DTS signal is affected by missing a high temperature reference point (hot bath). As a result, a workable data set from October to July is obtained.

The final temperature data collected are in good agreement with RBR probes. From the 10th of July until 15th, the FO-DTS temperatures recorded beneath the second bridge are correlated to the air temperature (Figure 3.3). We do not use this period for the interpretation.

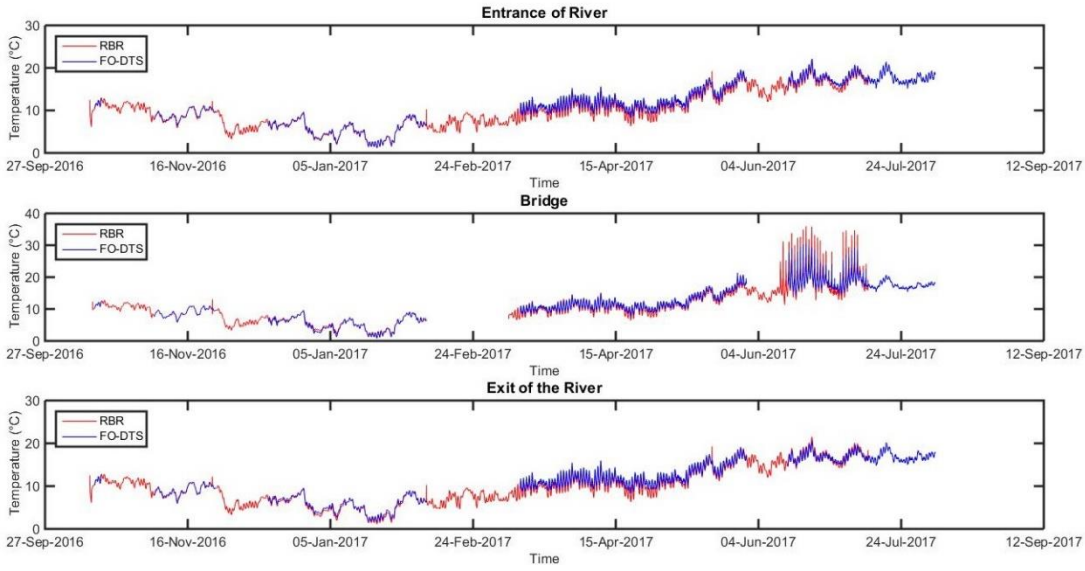

Figure 3.3: Validation of FO-DTS data for all periods. The gaps between the blue lines represent each period without record. The red lines represent RBR temperature record.

General description of the spatio-temporal variation of temperature

The Figure 3.4 shows the evaluation of the DTS temperatures in function of the distance and the time (Figure 3.4.a) and the monthly temperature averages as a function of distance (Figure 3.4.b). Figure 3.4.a represents all data collected during the survey period.

The temporal variation is mainly controlled by diurnal variation in daily frequency and seasonal changes in monthly variation. Note that the temperatures near the second bridge has a sharp evolution due to the low thickness of water in the river (Figure 3.4.b).

Mean temperatures in Winter season drop as low as 4.5°C in January. In summer, average temperatures are increasing up to 22°C. The second bridge has at least 3°C higher average temperatures in Spring and Summer seasons, and 1°C lower than average temperatures in Winter. The confluence is affecting the temperature recordings, though the temperature difference is not more than 0.5°C.

The median daily temperature amplitude is 0.91°C, whereas in certain days, it reaches up to 2.75°C. The 75 and 25 percentiles are ranging between 1.27°C, and 0.63°C. Physical references (bridge, confluence) indicate lower temperatures or higher temperatures than average throughout the monitoring period. Certain pools and riffles

deviates from the mean recorded temperatures throughout the monitoring period. These positions will be evaluated in detail in the upcoming section.

In December, and January temperatures recorded by FO-DTS is lower than $T_{aquifer}$ (Figure 2.3). During Spring months, temperature difference between the river and the aquifer is not as high as Winter months. In Summer, $T_{aquifer}$ is lower than temperatures recorded by FO-DTS.

Striking point in this plot (Figure 3.4) is the temperatures near second bridge, which are deviating greater than other temperature spots. The confluence is affecting temperatures in the studied area, although the effect is somewhat similar to a pool.

A decreasing trend in temperature is present in winter months towards downstream. The similar trend is not present in Spring, it is more or less flat. However, an increasing temperature trend is present towards downstream from May towards July. This is due to aquifer losing temperature towards upstream in Winter and gaining temperature in Summer.

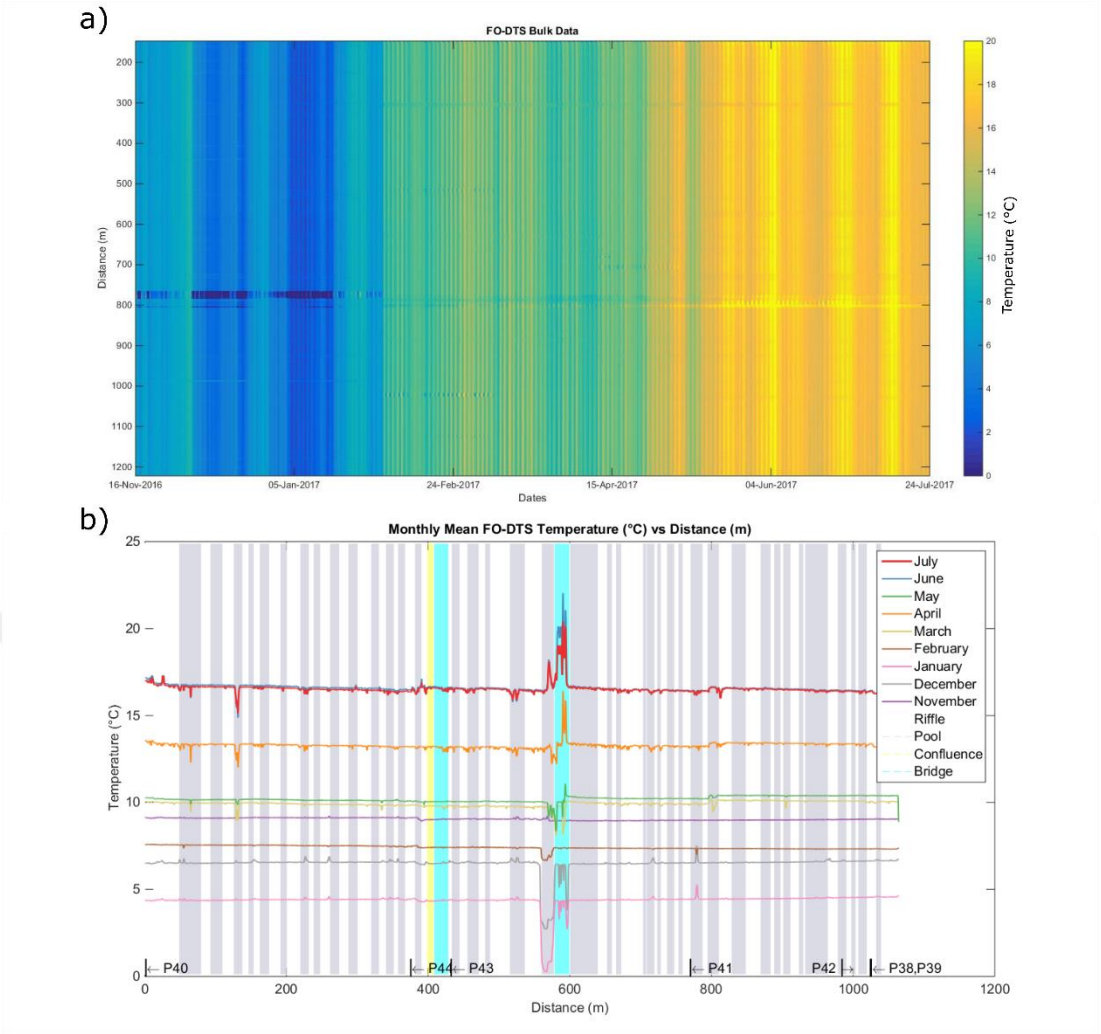

Figure 3.4: a) Temporal and spatial variation of the bulk FO-DTS data. The data is representing all the periods beginning from November until the early July. b) The plot of monthly temperature time series averages over distance. The white area is representing riffles, the grey shade represents pools. The yellow zone is confluence with concrete cascade. The turquoise color represents the bridges. The positions of mini-LOMOS stations are indicated at the bottom.

Effect of the pool and riffle

The positions of riffles have similar temperature averages. There is a relationship between the pools and temperature deviation from average. Pools have lower temperature in summer, and higher temperature in winter.

Deeper pools have higher temperature difference than mean temperature. In the case of Pool No. 6 (Table 5), is deeper than adjacent pools and in Summer months, its temperature is 2.5°C lower temperature than monthly T_{mean}. Contrary to Pool No. 6,

Pool No. 9 has 1 m depth, but, the temperature difference between the pool and monthly mean is not more than 0.2°C. In majority of the pools, a temperature difference is observable. Therefore, depths of pools are positively related with temperature differences within the river. However, only the depth is not sufficient to express the temperature difference, because as in the case of pool No. 9, having the largest depth, is warmer than a shallower pool No.6 (Figure 3.4.b).

During Spring and Summer months, pools have higher temperature deviation at downstream, than the pools upstream. However, in Winter, there are certain pools (pool No. 28 at 760 m, see Table 5) has higher temperature average than other pools. We do not see a similar higher temperature response than pool No. 6 or pool No. 9 for the same period.

Finally, downstream pools have higher temperature response than the pools upstream of second bridge. There is no certain difference in the shape or the slope of the pools between the ones downstream of bridge 2 and the ones upstream of bridge. Therefore, geometry is not the only dominant factor. This thermal response might be related to streambed topography and the heat capacity of the material accumulated towards downstream. Perhaps, the material brought by the confluence plays a higher role in determination of the temperature response.

A strong relationship between the slope of the pools and the temperature variation could not be found. However, the depth of pool affects the temperature deviation. There are also certain pools with higher temperature deviation even though depth is close to mean depth of the pools. This might be due to riverbed topography, or the accumulated high heat capacity material at the surface of the pool.

3.1.3 Temperature data from the mini-LOMOS

Temperature data from mini-LOMOS (Figure A.1 to Figure .8) is in good correlation with FO-DTS data ($\delta T<0.01^{\circ}C$). This means the recorded mini-LOMOS temperatures are validating the FO-DTS temperatures, as well as, the mini-LOMOS temperature recordings might be used for the validation of 2-D model. Temperatures recorded in Autumn (P38, P40), has at least 2°C lower temperature than $T_{aquifer}$. On the contrary, Temperatures recorded in Spring and Summer, has higher temperatures than $T_{aquifer}$.

Recorded temperature series vary both in diurnal variation and amplitude. The amplitude ranges between 0.5°C for P40 to 2.6°C for P42 for river temperatures. This difference is due to change in diurnal variation in different seasons. The amplitudes are lowering at least 60% at the deeper sensors. This is normal since the surface diurnal variation diminishes towards deeper zones. However, higher amplitude at deeper zones means the river is infiltrating towards the HZ (see Figure 2.1). The amplitude pattern changes for P42 between upper two temperature sensors and lower two temperature sensors. This might be due to inability of water to penetrate towards the HZ at deeper zones. There could be a clay limit after 20 cm. A phase shift is also present between temperature sensors in each location. For example, at station P40 (Figure .2), the sensor at 10 cm is at least 2°C above the temperature at 20 cm depth. This is due to a change in the lithology. Probably, a green clay dominant zone is present at this position.

Therefore, the temperature in the HZ is affected greatly by the spatial heterogeneity and the changes in the lithology are the dominant factor in this difference.

3.2 Estimation of Hydrothermal Parameters from Mini-LOMOS

The hydrothermal parameters of each mini-LOMOS stations are estimated by using an inversion script as detailed in section 2.3.1.b. In this section, the results of inversions, and water and heat fluxes will be investigated.

3.2.1 Inversion results

The results are validated by comparing the observed temperature series (Figure 3.5, see Figure A.1 to Figure B.6 for other stations). The RMSE of this position is 0.10 (Table 7). The results are in good correlation with the observed time series.

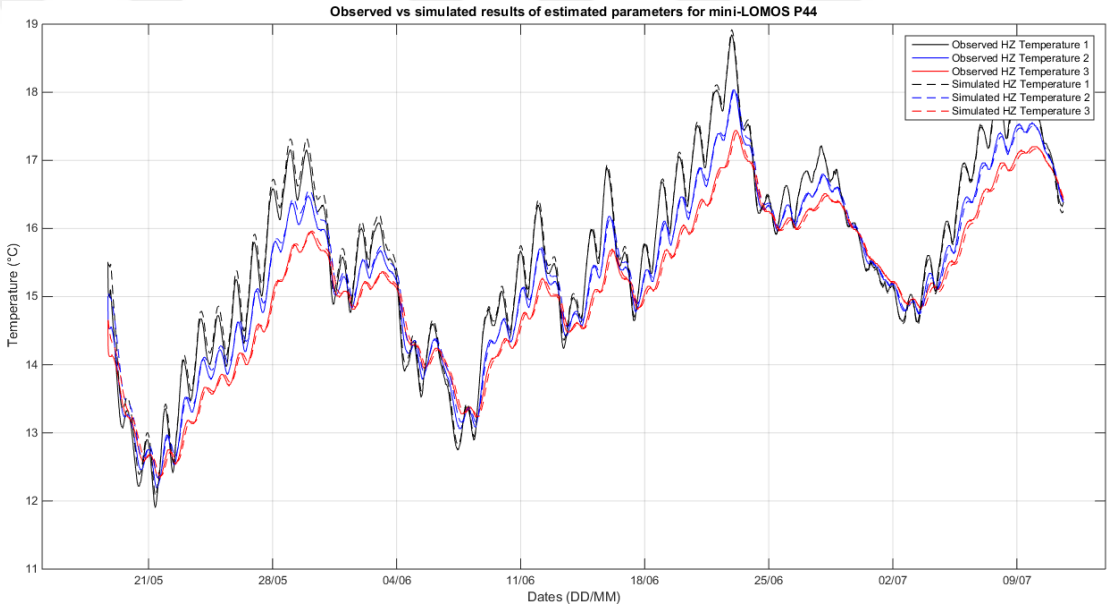

Figure 3.5: Simulated vs observed time series for mini-LOMOS station P44. Temperatures are recorded only for 5 days; the sensors are working fine. The statistical results of calibration are given in Table **7**.

The estimated parameters are stated in Table 6. The results vary up to an order of magnitude in between. Porosities (ω) range between 0.05 to 0.25. The highest porosity is at position P40. However, the porosity results are lower than the parameters from the literature (Table 3). Intrinsic permeability (λ) ranges between $0.10E^{-12}$ m to $0.50E^{-13}$ m. Intrinsic permeability and porosity are important physical parameters controlling the advective heat flow in the porous medium. Results of intrinsic

permeability is well within the range of literature values. The intrinsic permeability results are not so low, thus a certain amount of advective heat flow is normal.

Solid thermal conductivity parameters are within the literature parameters (Table 3). The estimated volume heat capacity results are ranging between 1500 $Jm^{-3}K^{-1}$ to 3500 $Jm^{-3}K^{-1}$.

Table 6: Parameters estimated after calibration

HZ Properties	Unit	P38-39	P40	P41	P42	P43	P44	P45	Clay
Porosity	-	0.05	0.25	0.10	0.10	0.15	0.10	0.05	0.05
Intrinsic Permeability	m^2	0.10E−12	0.10E−12	0.10E−13	0.10E−12	0.55E−12	0.55E−12	0.10E−12	0.50E−13
Solid thermal conductivity	$kgms^{-3}C^{-1}$	2.0	1.5	1.0	1.2	2.5	1.5	2.1	1.5
Solid thermal capacity	$Jkg^{-1}K^{-1}$	10^4	10^4	10^4	10^4	10^4	10^4	10^4	10^4
Specific Density	kgm^{-3}	2700	3500	1500	2500	1500	2200	3000	1900

The statistical results of the estimated parameters are shown in Table 7. RMSE is ranging between 0.03 to 0.47. The correlation of the results is very well. The position P42 has correlation coefficient 0.84. This might be due to fluctuation in the recorded temperature series at the bottom sensor.

Table 7: Statistical parameters of the estimated parameters for each mini-LOMOS station.

Statistical parameters	P38-39	P40	P41	P42	P43	P44	P45
RMSE	0.45	0.25	0.47	0.24	0.15	0.10	0.03
BIAS	0.33	0.13	0.02	-0.10	-0.08	-0.03	-0.01
RBIAS	0.03	0.01	0.00	-0.01	-0.01	0.00	-0.01
Correlation coefficient	0.97	0.98	0.91	0.84	0.99	0.99	1.00

3.2.2 Water and heat fluxes

Water and heat fluxes are estimated as represented in Figure 3.6 (see Figure C.1 to Figure C.5 for other stations). Water fluxes of P44 indicates that the dominant flow is infiltrating. There are only 2 brief periods where water is flowing to the river. Conductive flux in this station is following the diurnal temperature pattern. Though, in July, it fluctuates from the same pattern. This might be due to a disturbance in the probe. The advective fluxes are infiltrating. Contrary to the P44, the station P40 is exfiltrating. The station is positioned next to Bertin. Conductive fluxes are fluctuating in a random manner, rather than following diurnal pattern.

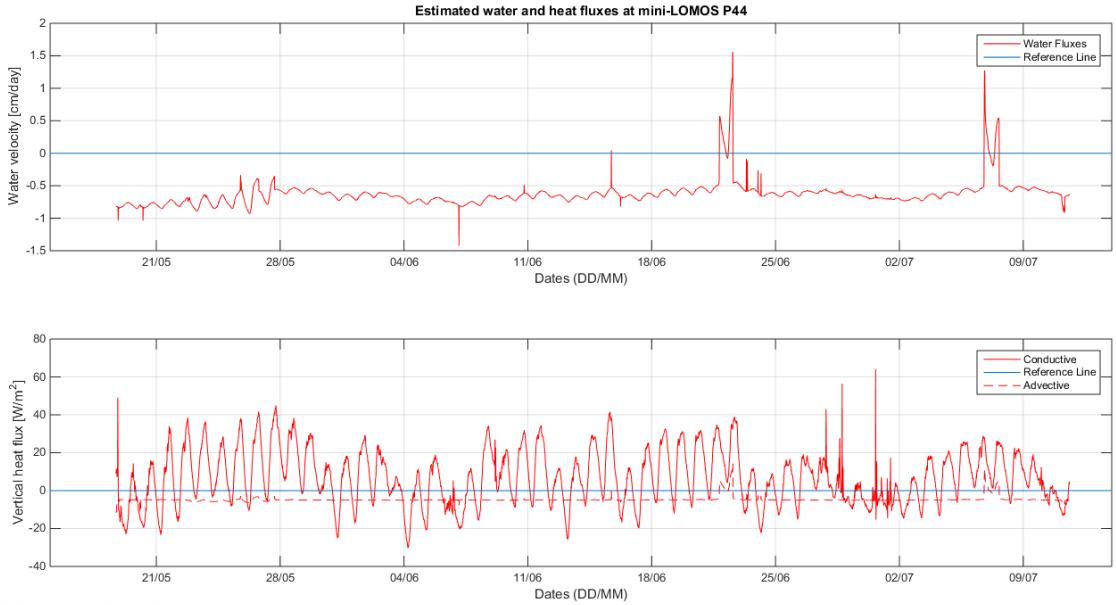

Figure 3.6: Estimated fluxes for the mini-LOMOS position P44. The minus sign indicates infiltration. The dominant advective flux is towards the HZ. The exfiltration is present only for 2 brief periods when the flux reversal is present. The water fluxes range between 1.5 cm/day to -1 cm/day.

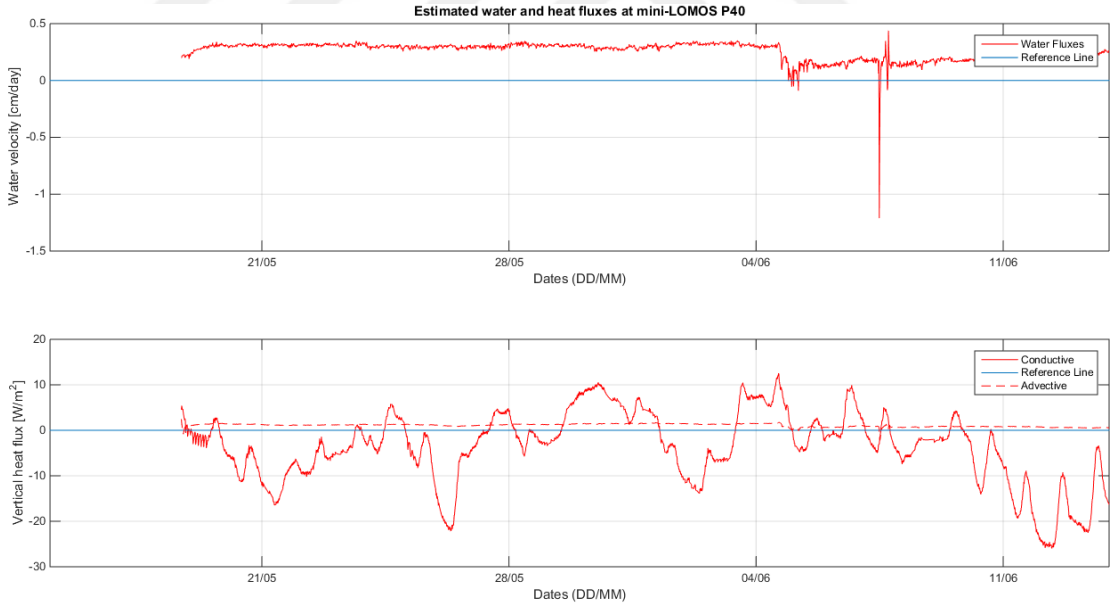

Figure 3.7: Estimated fluxes for the mini-LOMOS position P40. The minus sign indicates infiltration. Exfiltration is dominant in this station. Average water fluxes are 0.2 cm/day towards river. The

conductive fluxes are varying between +12 to -25 W/m^2. Advective fluxes are towards river, and they are decreasing with time.

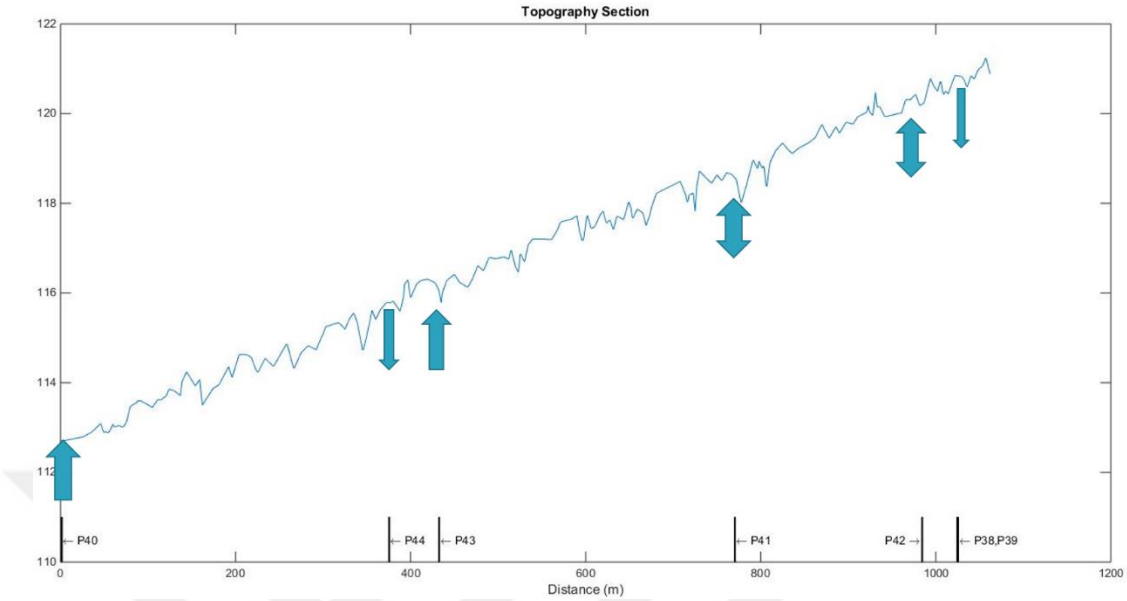

Figure 3.8: The plot of quantified water and heat fluxes of 1-D mini-LOMOS stations on the topography. The magnitude of dominant flows is represented by the thickness of the arrows.

The dominant flow is towards river at the upstream portion of the river. The downstream portion of the river is dominated by flow towards hyporheic zone (Figure 3.8). The exception for this are P44 and P38, P39. This might be because of lateral inflows or the relative positions of the mini-LOMOS stations to the riffle. If the station is at downstream part of riffle, the flow is expected to be dominant towards river, in the other hand, at the upstream portion: the flow is expected to be towards hyporheic zone (See Figure 1.1). Hence, downstream of river is gaining water, and upstream part of river is losing water according to the temperature recorded by the FO-DTS.

3.3 2-D Cross Section Model: Estimation of Water and Heat Fluxes

3.3.1 Comparison between the temperature time series

During Spring period, the temperature difference was as low as 0.2°C as in Figure 3.9. Overall, the temperatures are well represented except the deepest sensors (Figure 3.10). These sensors have an average RMSE of 0.30 from 1-D vertical inversion. The

temperature difference between 2-D and 1-D for these sensors can be explained in several ways. Firstly, the last sensor (where the RMSE is taken) is the boundary condition and the simulated temperatures might differ at the boundaries. Secondly, results of mini-LOMOS are for local scale 1-D vertical exchanges, therefore, 2-D exchanges are not taken into consideration, which might affect the results. Perhaps, these sensors are at the limit of the clay, which needs to be calibrated separately.

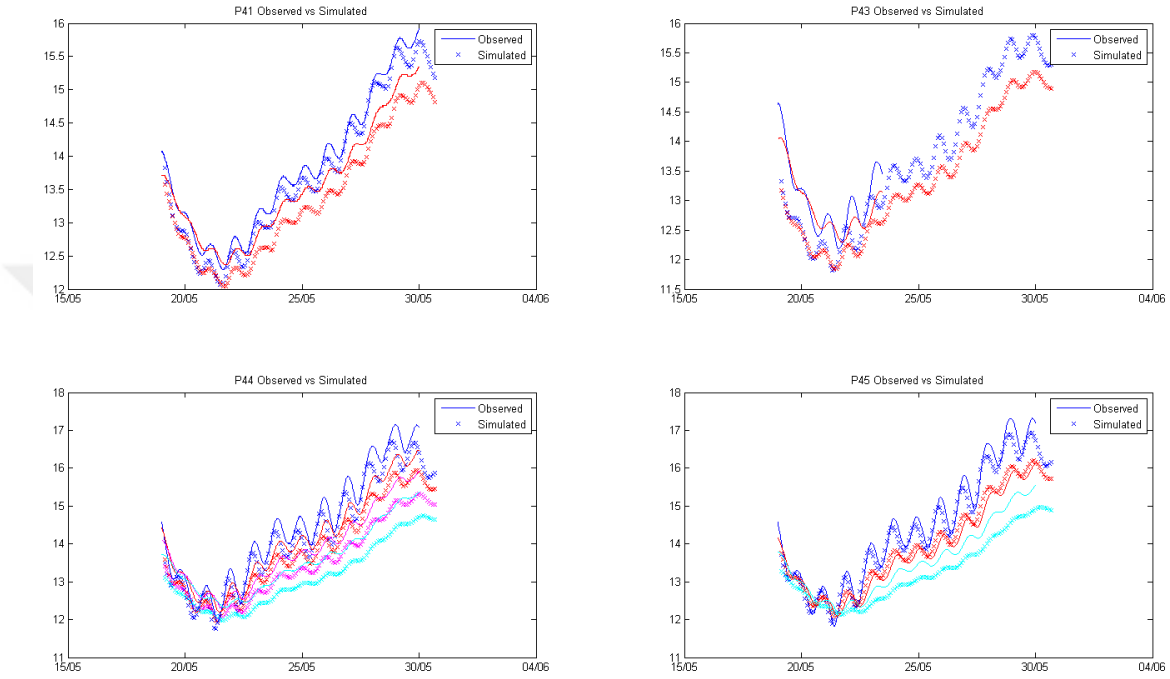

Figure 3.9: Comparison between observed mini-LOMOS temperature time series (thin lines) and simulated temperature time series from 2-D model (dots).

The model is responding well to Autumn season as well, and it is in good correlation with station P40 as can be seen in Figure 3.10. The temperature difference is below 0.2°C for Autumn, and head difference time series is also well correlated (Figure 3.10.b).

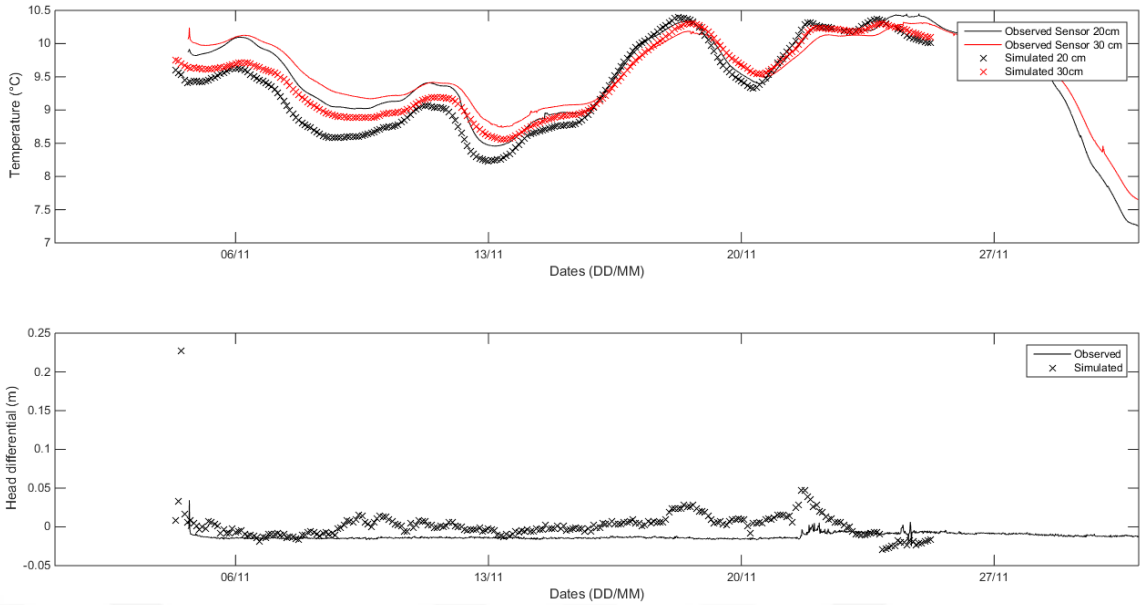

Figure 3.10: a) Comparison between observed mini-LOMOS temperature time series (thin lines) and simulated temperature time series from 2-D model (dots) for Autumn season. b) Comparison between head differential time series.

Overall, the simulated temperatures are in agreement with mini-LOMOS stations. The temperature difference is maximum 0.2°C for P43 station in Spring. The temperature difference 0.5°C created by the splice explains the difference between simulated and observed temperatures.

The parameters estimated for local scale processes and the results do not represent the whole lithological medium as spatial heterogeneity is high. Although, the results are representing the local processes, to simulate the water and heat fluxes in 2-D longitudinal, the estimated parameters are used as indicators for the zone variation in the 2-D mesh. Depending the position of the mini-LOMOS in the river, the dominant flow direction might change. Therefore, the high spatial heterogeneity and difficulty of estimating the parameters makes it harder to upscale the estimated parameters. However, FO-DTS data enables us to upscale the estimated parameters and develop a preliminary 2-D mesh to test the obtained parameters from mini-LOMOS studies.

3.3.2 Temporal variation of the temperature profile

Temporal variation of each season is shown in Figure 3.11. The results in the figure represent a snapshot of one run. Temperatures of aquifer in Autumn and Winter season

is above river temperature. Whereas, in Spring and Summer, temperatures of aquifer are above river temperature. A position at 600 m has 2°C lower temperature than average in Winter, and 2°C higher temperature than temperature average in Summer. This difference is not so obvious in transitional seasons such as Autumn or Spring.

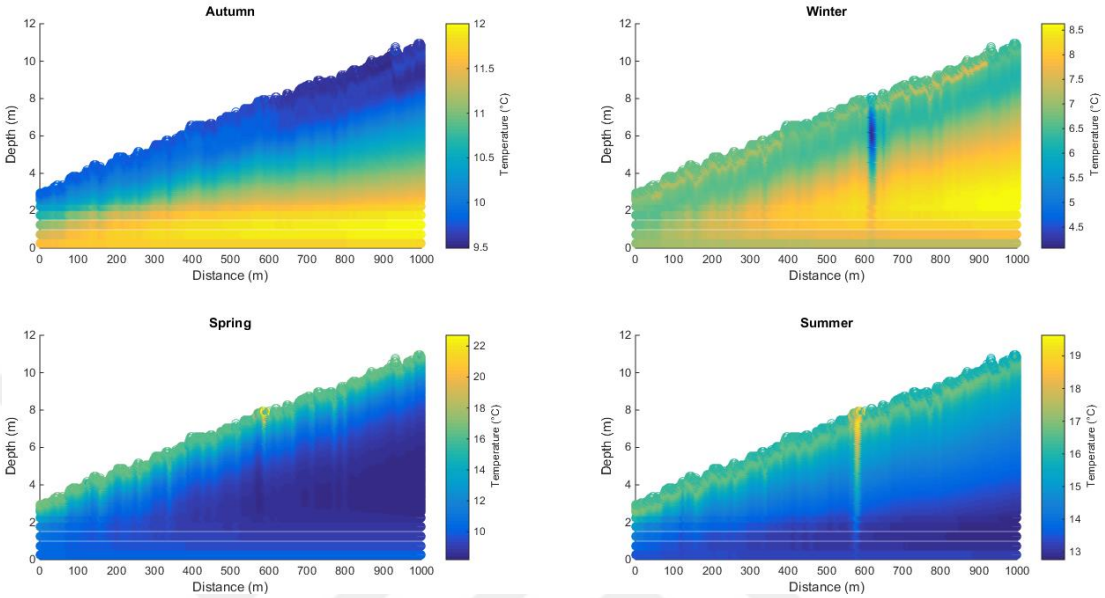

Figure 3.11: Seasonal variation of temperatures in 2-D model, a snapshot in time.

There is not a significant difference as in the variation of head levels (Figure D.1). This is due to imposed fixed head at the top boundary, and no flow boundary at the bottom. The head flow is lateral and decreasing gradually. In the upstream section in Winter season, there is a distinct zone with higher head, which coincides with a higher temperature zone during Winter (Figure 3.11).

3.3.3 Fluxes in 2-D and comparison to 1-D fluxes

The estimated fluxes for mini-LOMOS are quantified only for 1-D vertical fluxes. There might be 2-D fluxes present. Therefore, the advective and conductive fluxes might be affected by 2-D fluxes. Moreover, fluxes of P40 and P44 might be affected due to their position in riffles (Figure 1.1). If they are positioned downstream of the riffle, the exfiltration might be dominant, or if the station is positioned upstream part of the riffle, infiltration might be dominant.

2-D fluxes are estimated at the cells of mini-LOMOS stations to see the change between 1-D fluxes and 2-D fluxes. The water flux is fluctuating between 0.5 to - 1.5 cm/day. Water is both infiltrating and exfiltrating. Conductive fluxes are ranging between +5 to -5 W/m^2. The conductive fluxes follow the diurnal pattern. Advective fluxes are also flowing in both directions. There are certain periods where the fluxes reach up to 5 W/m^2.

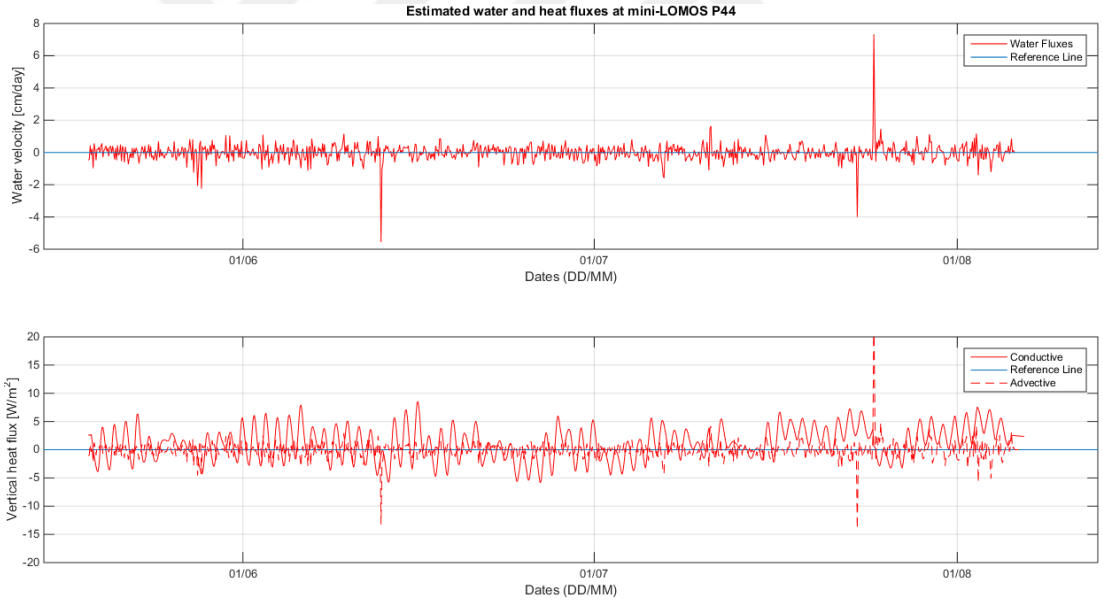

Figure 3.12: The estimated fluxes in P44.

The estimated fluxes from 2-D model deviate from the results of 1-D model (Figure 3.6, Figure 3.12). The estimated water fluxes in mini-LOMOS is dominantly towards HZ, however, 2-D water fluxes are in both directions without a dominant flow direction. The same pattern is present in advective fluxes. The magnitude of advective fluxes are lower than mini-LOMOS results, and in both directions.

The conductive fluxes show a similar pattern, yet, the amplitude of conductive fluxes is down by 90 %. This is due to presence of 2-D lateral fluxes as well as vertical fluxes.

The estimated fluxes for the 1-D hyporheic zone show temporal variation, conductive fluxes follow the diurnal pattern with varying magnitudes. The advective heat fluxes are closely related to the magnitude of the water fluxes. Diurnal variations in temperature are directly affecting the conductive fluxes. The important point is majority of the heat exchange is carried through conductive fluxes in the hyporheic zone.

The magnitude of the fluxes varies through seasons, as stations in Autumn has lower conductive and advective fluxes than in Spring stations. However, this is not validated by comparison of multi-seasonal temperature time series at the same position. Therefore, the result might be due to the spatial heterogeneity between the studied 1-D hyporheic columns.

2-D model fluxes have lower heat fluxes than the estimated heat fluxes of 1-D mini-LOMOS stations. The magnitude can change up to an order of magnitude. 1-D mini-LOMOS results indicate that the dominant advective fluxes are homogeneous in one direction (either infiltrating or exfiltrating). However, for the same positions, the advective fluxes does not have a dominant direction, and feeding both the river and hyporheic zone; resembling a pattern following the diurnal fluctuation of the conductive heat fluxes. This pattern is also present for the water fluxes.

This variation might be due to various reasons. The main reason is the head difference which is taken between aquifer and the river for the 2-D model, contrary to in-situ measurement of the head difference in the hyporheic zone for 1-D mini-LOMOS stations. Which is closely affecting the estimated advective fluxes. Another reason might be the resolution of the 2-D mesh. 1-D mini-LOMOS temperature time series is solved by a numerical model with 1 cm thick cells. However, 2-D mesh has 10 cm thick cells which creates a 1:10 cell ratio between the compared cells. Another possible reason is the 2-D lateral flows which were not considered in the 1-D mini-LOMOS results. This means some of the advective fluxes were lost to the lateral flow in the system. This case might be true for the conductive fluxes since their magnitude is also less than 1-D mini-LOMOS in 2-D mesh. Hyporheic exchange is noted to increase

during low flow conditions (Tonina and Buffington, 2007). Thus, increased flow rates in mini-LOMOS stations at Spring and Summer might be resulting from this fact.

The resolution difference between 2-D mesh and 1-D mini-LOMOS is due to limitations in the computing power. For the 2-D model, it takes around 10 minutes per run, depending on the length of time series. However, a finer 2-D model would require much more computing power. Since the ratio of cells is 1:10, imitating the same resolution with 1-D mini-LOMOS would be impractical.

3.4 Relationships Among Streambed Temperatures and Geometry of the Pool

Pools and riffles, geometry of the pool is closely related with the temperature variance in the river, as well as the interactions with banks and other physical references such as bridges, concrete slabs etc. The variation of the pool and riffle sequences in amplitude, size and geometry are not the only key factors driving the hyporheic exchange.

They act as a storage of heat and respond slower to diurnal temperature variations than riffles. The heat difference between pools and adjacent riffles reach up to 2.5°C.

As can be seen in Figure 3.13, the temperatures are lower than the average temperature of the river in Spring and Summer (See Figure 3.11). These temperatures are around 14.5°C to 15°C at the center of the pool, while they are increasing to 16°C. The similar temperature difference is not present in Autumn season. But the temperature difference is beginning to increase in Winter. This result is in agreement with the monthly temperature variation (See Figure 3.4.b). Therefore, only the depth or the geometry of the pool is not sufficient to explain the difference in the temperatures. There are flooding events present in earlier February, and in March (see Figure 2.3). A possible alteration of the streambed topography and the lithology might be the reason for this difference in response. A more detailed study of the pools is required to understand the reason.

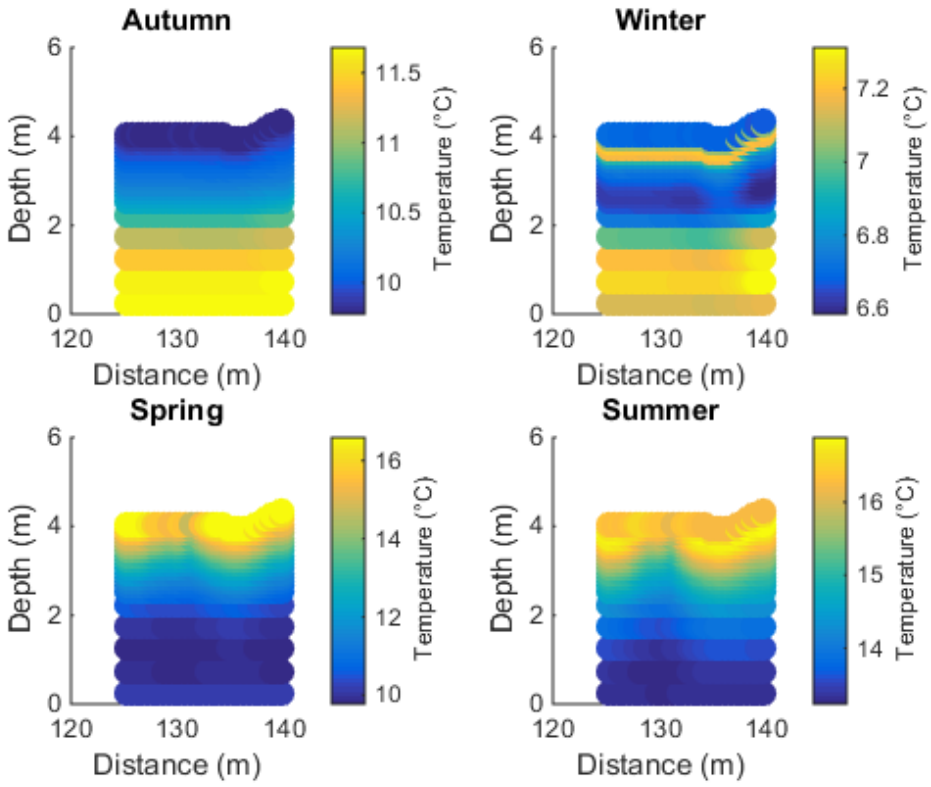

Figure 3.13: The 2-D temperature variation of the pool No.9 per season. A drop in temperature is observable in Spring and Summer.

4. CONCLUSION AND PERSPECTIVES

The temperature and head data acquired are validated and in good correlation between each other. The estimated hydro-thermal parameters are well within the literature ranges (Table 3). The limitation of the hydro-thermal parameters obtained is that we obtain information only about the 1-D vertical heterogeneity. However, the spatial heterogeneity is variable and can change up to an order of magnitude from location to location.

A more detailed study is needed for the relationship of the fluxes and the riffle system. The study lacks the installation of the mini-LOMOS into pool systems because of their depth. This is due to physical limitations on the deployment of the tool (Cucchi et al., 2018).

The spatial variation of temperature time series is high. The heterogeneity is great due to the abundance of the pool and riffle sequences, and physical references (i.e. bridge, confluence, concrete slab). The decreasing and increasing temperature trend during different seasons is due to losing stream condition at the upstream section of the hydrologic network and gaining stream condition at the downstream section of the hydrologic network. This is also supported by the estimated fluxes by the mini-LOMOS.

The methodology used in this study has strengths and weaknesses. FO-DTS provides very fine and accurate temperature data as well as mini-LOMOS. The estimated parameter set is robust for 1-D hyporheic zone exchanges, and they are in good agreement with the literature values. However, the results are explaining for local scale exchanges, and these exchanges are subject to spatial variation of the lithology. However, mini-LOMOS is a strong tool for estimating the 1-D fluxes at local scales.

Up-scaling the results, 2-D mesh is also subject to spatial variation and the mini-LOMOS parameters are too few to represent whole length of the studied zone. This challenge might be overcome by deployment of more mini-LOMOS stations and increasing the abundance of the physical parameters estimated for the studied medium. The resolution of the 2-D model is sufficient to explain the exchanges. However, it is not in the same resolution of 1-D model. This can be improved with the increased

computing power. For practical reasons, the resolution is good for analyzing the fluxes at this scale.

The 2-D model is used to simulate the heat and water fluxes with the help of FO-DTS data set. The data set used in the model is validated and the model provides good results. The temperature variation of the hyporheic column can be observed with the variation of the FO-DTS data. The hydro-thermal parameters are picked depending on the mini-LOMOS parameters and the proximity of mini-LOMOS stations with each other and their parameters. This approach comes handy to initiate the model and solve the system. But in a 1 km reach scale numerical model, the spatial heterogeneity is very high and depends on many factors (i.e. pool and riffle, geometry, lithology). Therefore, additional refinement with more mini-LOMOS stations is required to overcome the problem of spatial heterogeneity. This might result in additional zones and increased accuracy of the developed 2-D model.

To conclude, this thesis presents a new combination of methods for characterization of the surface water-ground water interactions. High-resolution spatial and temporal temperature measurement unit FO-DTS is combined with mini-LOMOS and a 2-D mesh is developed to express the hyporheic exchange at reach scale. According to the conclusions, answers are sought for the research objectives of the study.

– Is it possible to use the hydro-thermal parameters estimated with a 1-D model in a 2-D model at reach scale?

The estimated hydro-thermal parameters from the 1-D model provide good data set for the 2-D model. The results are in good agreement with the mini-LOMOS results. It is refined for the Spring season and validated for Autumn season. However, more verification is needed for the parameters. Spatial heterogeneity problem requires additional surveys to estimate the parameters. Coupling FO-DTS with piezometric and temperature data from the study area to estimate fluxes and validating with mini-LOMOS possess a high potential for future research and up-scaling the parameters for the use of water managers.

– Are we able to represent the effects of pool and riffle sequences without data set?

The FO-DTS unit detects the spatial variations on temperature resulted from pool and riffle sequences. However, the spatial variation is not just resulted from these

sequences. Mini-LOMOS is a strong tool for characterization of the 1-D local scale exchanges. Coupling both methods provides insight about the effect of pool and riffle sequences. The geometry of the pool and riffle sequences are important factors on the exchanges. A detailed study should be taken to further analyze the effect of pool and riffle sequences by addressing the effect of other factors correctly.

5. REFERENCES

Allan, J. D., Ibañez Castillo, M. M. (2009) *Stream Ecology : Structure and Function of Running Waters*, 2nd Edition. Springer, Dordrecht, oCLC : 837704805.

Anderson, M. P., (2005) Heat as a Ground Water Tracer. *Ground Water* 43 (6), 951–968.

Baratelli, F., Flipo, N., Moatar, F. (2016) Estimation of stream-aquifer exchanges at regional scale using a distributed model : Sensitivity to in-stream water level fluctuations, riverbed elevation and roughness. *Journal of Hydrology* 542, 686–703.

Bejan, A. (2013) *Convection Heat Transfer*. John Wiley & Sons.

Berrhouma, A. (2016) Estimation des flux d'énergie à l'interface nappe-rivière des Avenelles. *PIREN-Seine*-Phase VII-Rapport.

Boano, F., Harvey, J. W., Marion, A., Packman, A. I., Revelli, R., Ridolfi, L., Wörman, A. (2014) Hyporheic flow and transport processes : Mechanisms, models, and biogeochemical implications. *Reviews of Geophysics* 52 (4), 603–679.

Boulêtreau, S., Salvo, E., Lyautey, E., Mastrorillo, S., Garabetian, F. (2012) Temperature dependence of denitrification in phototrophic river biofilms. *Science of The Total Environment* 416, 323–328.

Boulton, A. J., Findlay, S., Marmonier, P., Stanley, E. H., Valett, H. M. (1998) The functional significance of the hyporheic zone in streams and rivers. *Annual Review of Ecology and Systematics* 29 (1), 59–81.

Bray, E. N., Dunne, T. (2017) Observations of bedload transport in a gravel bed river during high flow using fiber-optic DTS methods : Bedload transport and disentrainment using dts methods. *Earth Surface Processes and Landforms* 42 (13), 2184–2198.

Bredehoeft, J. D., Papaopulos, I. S. (1965) Rates of vertical groundwater movement estimated from the Earth's thermal profile. *Water Resources Research* 1 (2), 325–328.

Briggs, M. A., Lautz, L. K., McKenzie, J. M. (2012) A comparison of fibre-optic distributed temperature sensing to traditional methods of evaluating groundwater inflow to streams. *Hydrological Processes* 26 (9), 1277–1290.

Cardenas, M. B., Zlotnik, V. A. (2003) Three-dimensional model of modern channel bend deposits. *Water Resources Research* 39 (6).

Chen, X. (2000) Measurement of streambed hydraulic conductivity and its anisotropy. *Environmental Geology* 39 (12), 1317–1324.

Chery, L., de Marsily, G. (Eds.) (2007) *Aquifer Systems Management : Darcy's Legacy in a World of Impending Water Shortage.* No. 10 in International Association of Hydrogeologists selected papers. Taylor & Francis, London; New York, oCLC : ocn122701640.

Constantz, J. (1998) Interaction between stream temperature, streamflow, and groundwater exchanges in alpine streams. *Water Resources Research* 34 (7), 1609–1615.

Constantz, J. (2008) Heat as a tracer to determine streambed water exchanges : Heat used to determine streambed water exchanges. *Water Resources Research* 44 (4).

Cucchi, K., Rivière, A., Baudin, A., Berrhouma, A., Durand, V., Rejiba, F., Rubin, Y., Flipo, N. (2018) LOMOS-mini : A coupled system quantifying transient water and heat exchanges in streambeds. *Journal of Hydrology* 561, 1037–1047.

de Marsily, G. (1986) *Quantitative Hydrogeology : Groundwater Hydrology for Engineers*. Academic Press.

Eppelbaum, L., Kutasov, I., Pilchin, A. (2014) *Applied Geothermics*. Springer Science & Business.

Fetter, C. W. (2001) *Applied Hydrogeology*. Prentice Hall.

Flipo, N. (2013) *Modélisation des Hydrosystèmes Continentaux pour une Gestion Durable de la Ressource en Eau*. PhD Thesis, Université Pierre et Marie Curie-Paris VI.

Flipo, N., Monteil, C., Poulin, M., de Fouquet, C., Krimissa, M. (2012) Hybrid fitting of a hydrosystem model : Long-term insight into the Beauce aquifer functioning (France). *Water Resources Research* 48 (5).

Flipo, N., Mouhri, A., Labarthe, B., Biancamaria, S., Rivière, A., Weill, P. (2014) Continental hydrosystem modelling : The concept of nested stream-aquifer interfaces. *Hydrology and Earth System Sciences* 18 (8), 3121–3149.

Hatch, C. E., Fisher, A. T., Revenaugh, J. S., Constantz, J., Ruehl, C. (2006) Quantifying surface water-groundwater interactions using time series analysis of streambed thermal records : Method development. *Water Resources Research* 42 (10).

Hausner, M. B., Suárez, F., Glander, K. E., van de Giesen, N., Selker, J. S., Tyler, S. W. (2011) Calibrating Single-Ended Fiber-Optic Raman Spectra Distributed Temperature Sensing Data. *Sensors* 11 (11), 10859–10879.

Hayashi, M., Rosenberry, D. O. (2002) Effects of Ground Water Exchange on the Hydrology and Ecology of Surface Water. *Groundwater* 40 (3), 309–316.

Huang, X., Andrews, C. B., Liu, J., Yao, Y., Liu, C., Tyler, S. W., Selker, J. S., Zheng, C. (2016) Assimilation of temperature and hydraulic gradients for quantifying the spatial variability of streambed hydraulics. *Water Resources Research* 52 (8), 6419–6439.

Kalbus, E., Reinstorf, F., Schirmer, M. (2006) Measuring methods for groundwater - surface water interactions : A review. *Hydrology and Earth System Sciences* 10 (6), 873–887.

Keery, J., Binley, A., Crook, N., Smith, J. W. (2007) Temporal and spatial variability of groundwater–surface water fluxes : Development and application of an analytical method using temperature time series. *Journal of Hydrology* 336 (1-2), 1–16.

Kurtulus, B., Flipo, N., Goblet, P., Vilain, G., Tournebize, J., Tallec, G. (2011) Hydraulic Head Interpolation in an Aquifer Unit Using ANFIS and Ordinary Kriging. In : Kacprzyk, J., Madani, K., Correia, A. D., Rosa, A., Filipe, J. (Eds.), *Computational Intelligence*. Vol. 343. Springer Berlin Heidelberg, Berlin, Heidelberg, pp. 265–276.

Lowry, C. S., Walker, J. F., Hunt, R. J., Anderson, M. P. (2007) Identifying spatial variability of groundwater discharge in a wetland stream using a distributed temperature sensor. *Water Resources Research* 43 (10).

Mathers, K. L., Hill, M. J., Wood, P. J. (2017) Benthic and hyporheic macroinvertebrate distribution within the heads and tails of riffles during baseflow conditions. *Hydrobiologia* 794 (1), 17–30.

MathWorks (2018) *MATLAB*. https ://www.mathworks.com/products/matlab.html.

Menichino, G. T., Hester, E. T. (2014) Hydraulic and thermal effects of in-stream structure-induced hyporheic exchange across a range of hydraulic conductivities. *Water Resources Research* 50 (6), 4643–4661.

Mouhri, A., Flipo, N., Rejiba, F., de Fouquet, C., Bodet, L., Kurtulus, B., Tallec, G., Durand, V., Jost, A., Ansart, P., Goblet, P. (2013) Designing a multi-scale sampling system of stream–aquifer interfaces in a sedimentary basin. *Journal of Hydrology* 504, 194–206.

Munz, M., Oswald, S. E., Schmidt, C. (2016) Analysis of riverbed temperatures to determine the geometry of subsurface water flow around in-stream geomorphological structures. *Journal of Hydrology* 539, 74–87.

Newcomer, M. E., Hubbard, S. S., Fleckenstein, J. H., Maier, U., Schmidt, C., Thullner, M., Ulrich, C., Flipo, N., Rubin, Y. (2016) Simulating bioclogging effects on dynamic riverbed permeability and infiltration. *Water Resources Research* 52 (4), 2883–2900.

Onderka, M., Banzhaf, S., Scheytt, T., Krein, A. (2013) Seepage velocities derived from thermal records using wavelet analysis. *Journal of Hydrology* 479, 64–74.

PIREN-Seine (2018) Programme Interdisciplinaire de Recherche sur l'eau et l'environnement du bassin de la Seine. https://www.piren-seine.fr/.

Poole, G. C., Berman, C. H. (2001) An Ecological Perspective on In-Stream Temperature : Natural Heat Dynamics and Mechanisms of Human-Caused Thermal Degradation. *Environmental Management* 27 (6), 787–802.

Poole, G. C., O'Daniel, S. J., Jones, K. L., Woessner, W. W., Bernhardt, E. S., Helton, A. M., Stanford, J. A., Boer, B. R., Beechie, T. J. (2008) Hydrologic spiralling : The role of multiple interactive flow paths in stream ecosystems. *River Research and Applications* 24 (7), 1018–1031.

Pryet, A., Labarthe, B., Saleh, F., Akopian, M., Flipo, N. (2015) Reporting of Stream-Aquifer Flow Distribution at the Regional Scale with a Distributed Process-Based Model. *Water Resources Management* 29 (1), 139–159.

Read, T., Bense, V. F., Hochreutener, R., Bour, O., Le Borgne, T., Lavenant, N., Selker, J. S. (2015) Thermal-plume fibre optic tracking (T-POT) test for flow velocity measurement in groundwater boreholes. *Geoscientific Instrumentation, Methods and Data Systems* 4 (2), 197–202.

Read, T., Bour, O., Selker, J. S., Bense, V. F., Borgne, T. L., Hochreutener, R., Lavenant, N. (2014) Active-distributed temperature sensing to continuously quantify vertical flow in boreholes. *Water Resources Research* 50 (5), 3706–3713.

Rivière, A., Gonçalvès, J., Jost, A., Font, M. (2014) Experimental and numerical assessment of transient stream–aquifer exchange during disconnection. *Journal of Hydrology* 517, 574–583.

Rosenberry, D. O., Briggs, M. A., Voytek, E. B., Lane, J. W. (2016) Influence of groundwater on distribution of dwarf wedgemussels (Alasmidonta heterodon) in the upper reaches of the Delaware River, northeastern USA. *Hydrology and Earth System Sciences* 20 (10), 4323–4339.

Saleh, F., Flipo, N., Habets, F., Ducharne, A., Oudin, L., Viennot, P., Ledoux, E., (2011) Modeling the impact of in-stream water level fluctuations on stream-aquifer interactions at the regional scale. *Journal of Hydrology* 400 (3-4), 490–500.

Schmidt, C., Conant, B., Bayer-Raich, M., Schirmer, M. (2007) Evaluation and field-scale application of an analytical method to quantify groundwater discharge using mapped streambed temperatures. *Journal of Hydrology* 347 (3-4), 292–307.

Selker, J. S., Thévenaz, L., Huwald, H., Mallet, A., Luxemburg, W., van de Giesen, N., Stejskal, M., Zeman, J., Westhoff, M., Parlange, M. B. (2006a) Distributed fiber-optic temperature sensing for hydrologic systems. *Water Resources Research* 42 (12).

Selker, J. S., van de Giesen, N., Westhoff, M., Luxemburg, W., Parlange, M. B. (2006b) Fiber optics opens window on stream dynamics. *Geophysical Research Letters* 33 (24).

Silliman, S. E., Booth, D. F. (1993) Analysis of time-series measurements of sediment temperature for identification of gaining vs. losing portions of Juday Creek, Indiana. *Journal of Hydrology* 146, 131–148.

Stallman, R. W. (1965) Steady one-dimensional fluid flow in a semi-infinite porous medium with sinusoidal surface temperature. *Journal of Geophysical Research* 70 (12), 2821–2827.

Stonestrom, D. A., Constantz, J. (Eds.) (2003) *Heat as a Tool for Studying the Movement of Ground Water near Streams*. No. 1260 in Circular / U. S. Department of the Interior, U.S. Geological Survey. U.S. Geological Survey, Information Services, Reston, Va, oCLC : 249104967.

Suzuki, S. (1960) Percolation measurements based on heat flow through soil with special reference to paddy fields. *Journal of Geophysical Research* 65 (9), 2883–2885.

Tallec, G., Ansart, P., Guérin, A., Delaigue, O., Blanchouin, A. (2015) Observatoire Oracle.

Tonina, D., Buffington, J. M. (2007) Hyporheic exchange in gravel bed rivers with pool-riffle morphology : Laboratory experiments and three-dimensional modeling. *Water Resources Research* 43 (1).

Trauth, N., Schmidt, C., Vieweg, M., Maier, U., Fleckenstein, J. H. (2014) Hyporheic transport and biogeochemical reactions in pool-riffle systems under varying ambient groundwater flow conditions. *Journal of Geophysical Research : Biogeosciences* 119 (5), 910–928.

Tyler, S. W., Selker, J. S., Hausner, M. B., Hatch, C. E., Torgersen, T., Thodal, C. E., Schladow, S. G. (2009) Environmental temperature sensing using Raman spectra DTS fiber-optic methods. *Water Resources Research* 45 (4).

van de Giesen, N., Steele-Dunne, S. C., Jansen, J., Hoes, O., Hausner, M. B., Tyler, S., Selker, J. (2012) Double-Ended Calibration of Fiber-Optic Raman Spectra Distributed Temperature Sensing Data. *Sensors* 12 (5), 5471–5485.

Vieweg, M., Kurz, M. J., Trauth, N., Fleckenstein, J. H., Musolff, A., Schmidt, C. (2016) Estimating time-variable aerobic respiration in the streambed by combining electrical conductivity and dissolved oxygen time series : Variable Respiration in the Streambed. *Journal of Geophysical Research : Biogeosciences* 121 (8), 2199–2215.

Vogt, T., Schneider, P., Hahn-Woernle, L., Cirpka, O. A. (2010) Estimation of seepage rates in a losing stream by means of fiber-optic high-resolution vertical temperature profiling. *Journal of Hydrology* 380 (1-2), 154–164.

Waples, D. W., Waples, J. S. (2004) A Review and Evaluation of Specific Heat Capacities of Rocks, Minerals, and Subsurface Fluids. Part 1 : Minerals and Nonporous Rocks. *Natural Resources Research* 13 (2), 97–122.

White, D. S. (1990) Biological relationships to convective flow patterns within stream beds. *Hydrobiologia* 196 (2), 149–158.

Yao, Y., Huang, X., Liu, J., Zheng, C., He, X., Liu, C. (2015) Spatiotemporal variation of river temperature as a predictor of groundwater/surface-water interactions in an arid watershed in China. *Hydrogeology Journal* 23 (5), 999–1007.

Zheng, L. (2017) *Nitrate removal efficiency in hyporheic zones : The effect of temperature and bedform dynamics*. Thesis.

APPENDICES

Appendix A. Mini-LOMOS

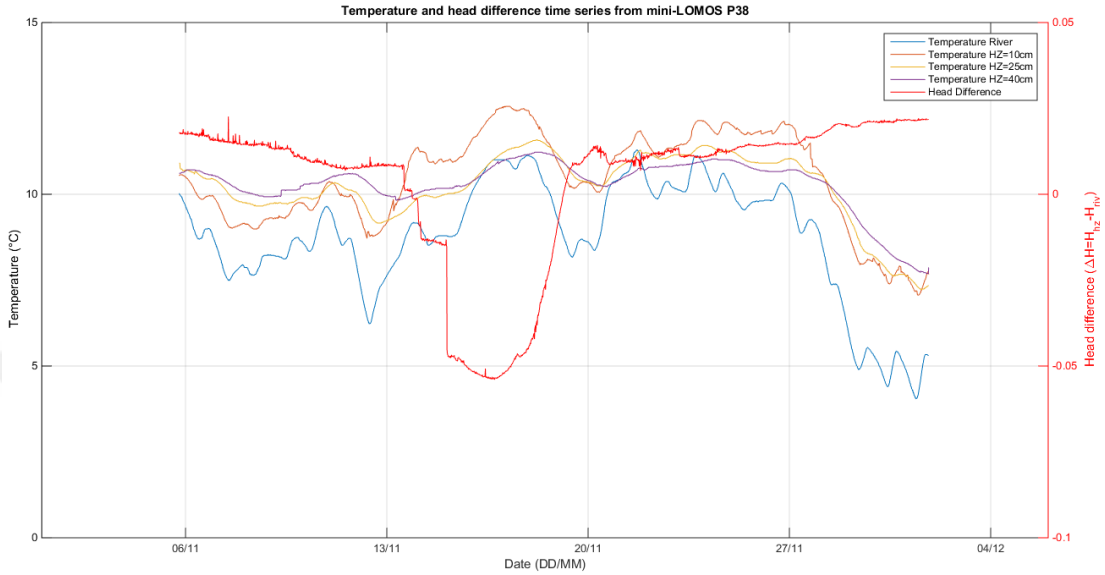

Figure A.1: Temperature and head difference time series of mini-LOMOS station P38, this station recorded in Winter season. Red line represents the head difference, and other lines are from each sensor at various depth. The location is at upstream part of study area, at 1034 m from Bertin. This station is not included in the 2-D model since its outside of the modeled zone. Dominant water flux is upstream except a week between 13-20 November.

Appendix A continue

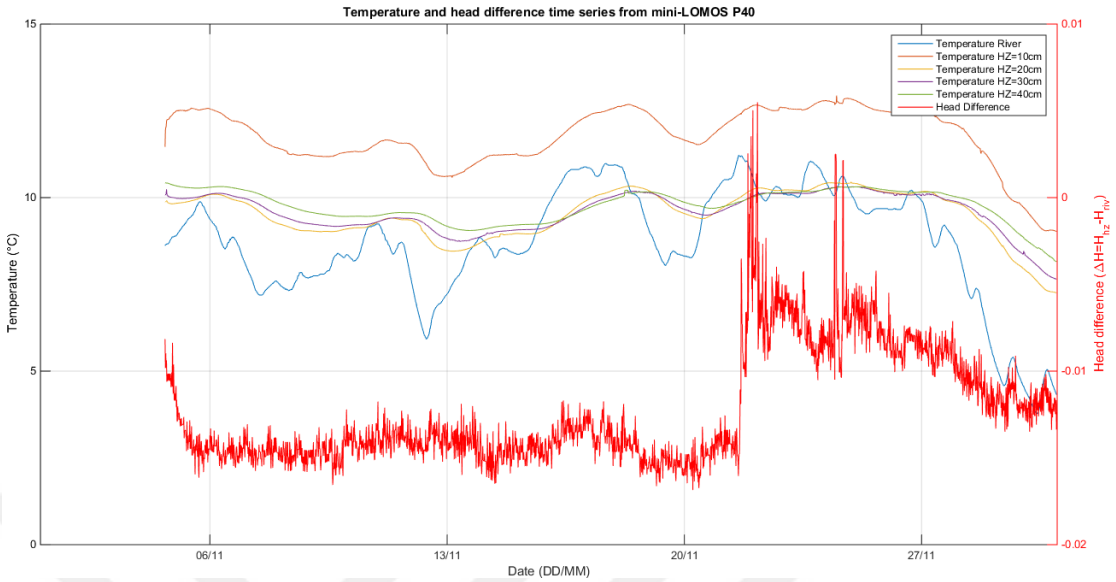

Figure .2: Temperature and head difference time series of mini-LOMOS station P40, this station recorded in Winter season. Red line represents the head difference, and other lines are from each sensor at various depth. The location is next to Bertin station. Fluctuation of head difference is higher than other positions. The dominant flux is towards hyporheic zone. All sensors recorded temperature data.

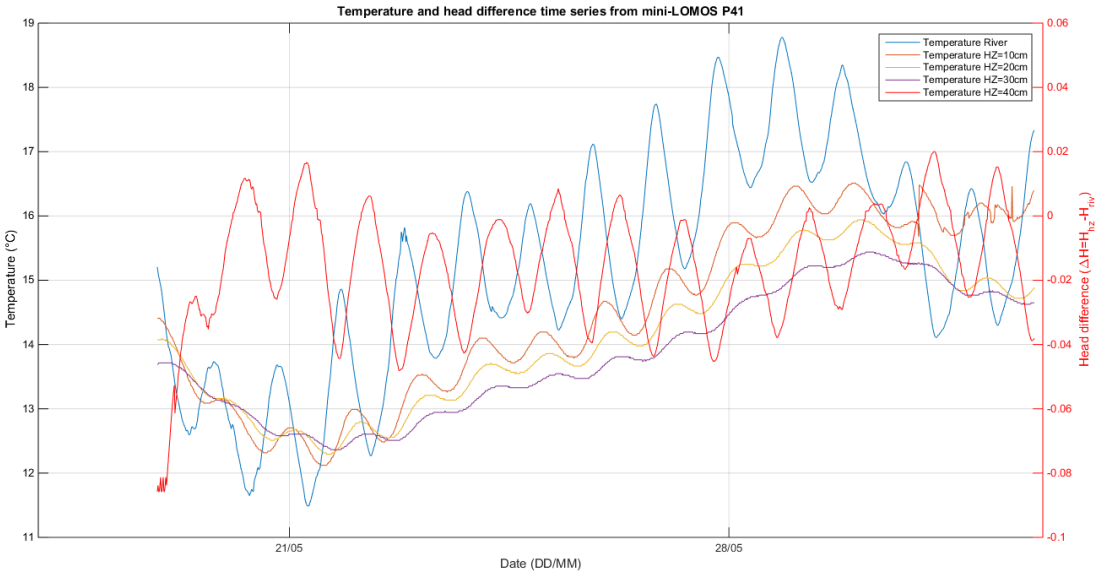

Figure .3: Temperature and head difference time series of mini-LOMOS station P41, this station recorded in Spring season. Red line represents the head difference, and other lines are from each sensor at various depth. The location is at 774 m. The dominant water flux is towards hyporheic zone. All sensors recorded temperature data. However, the deepest temperature sensor recorded faulty data, thus omitted.

Appendix A continue

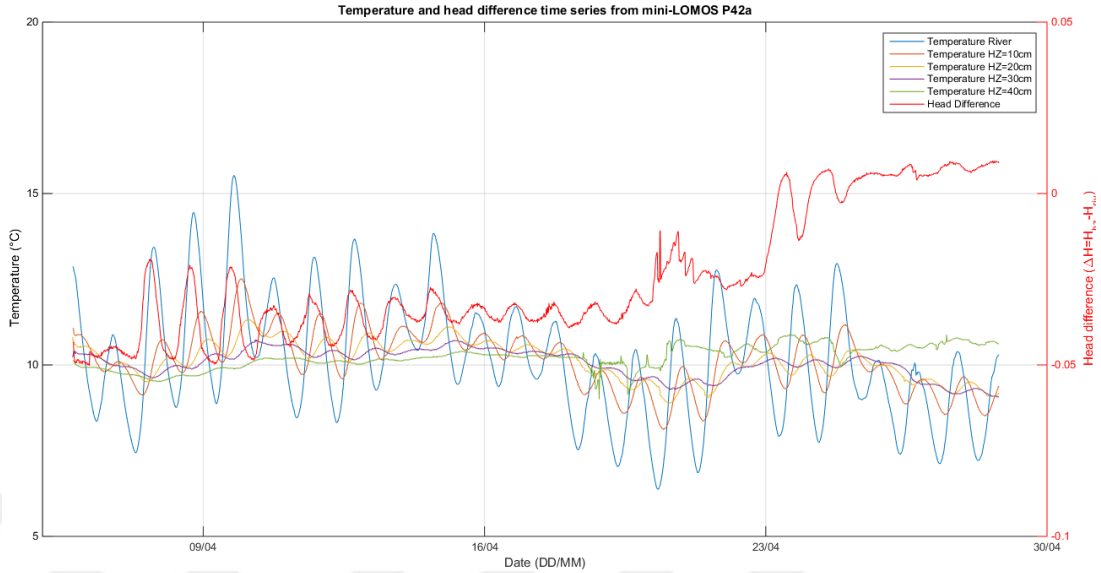

Figure .4: Temperature and head difference time series of mini-LOMOS station P42a, this station recorded in Spring season. Red line represents the head difference, and other lines are from each sensor at various depth. The location is at 994 m. The dominant water flux is towards hyporheic zone. After 23 April, the water flux reverses, and flows into river. The temperature sensor at 40 cm depth deviates from the actual temperatures, it might have been damaged.

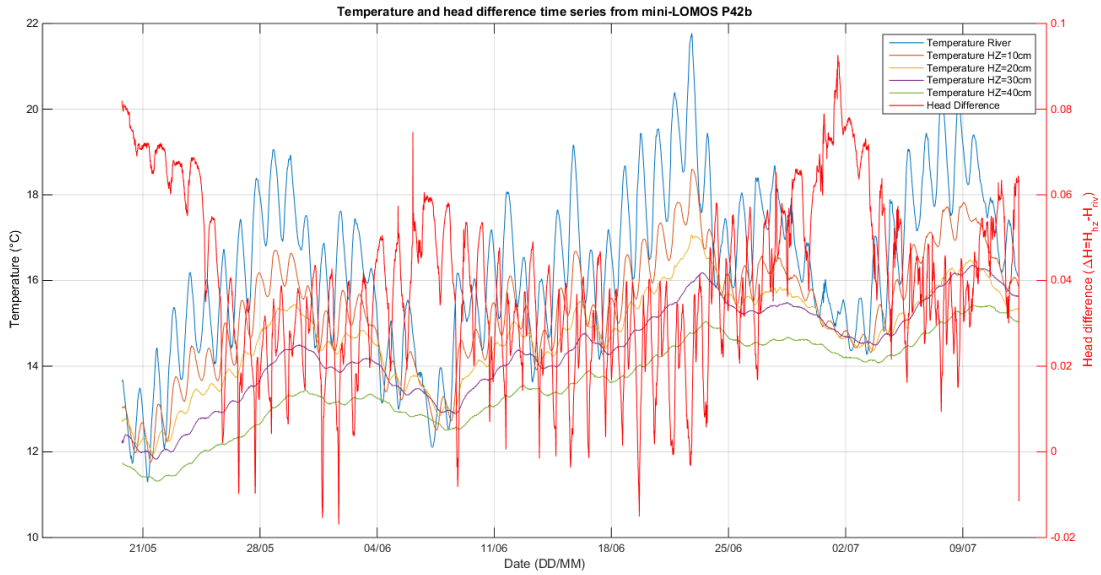

Figure .5: Temperature and head difference time series of mini-LOMOS station P42b, this station recorded in Summer season. Red line represents the head difference, and other lines are from each sensor at various depth. The location is at 994 m. The dominant water flux is towards river. Temperature sensors are not damaged; however, the amplitude head difference is higher than other positions.

Appendix A continue

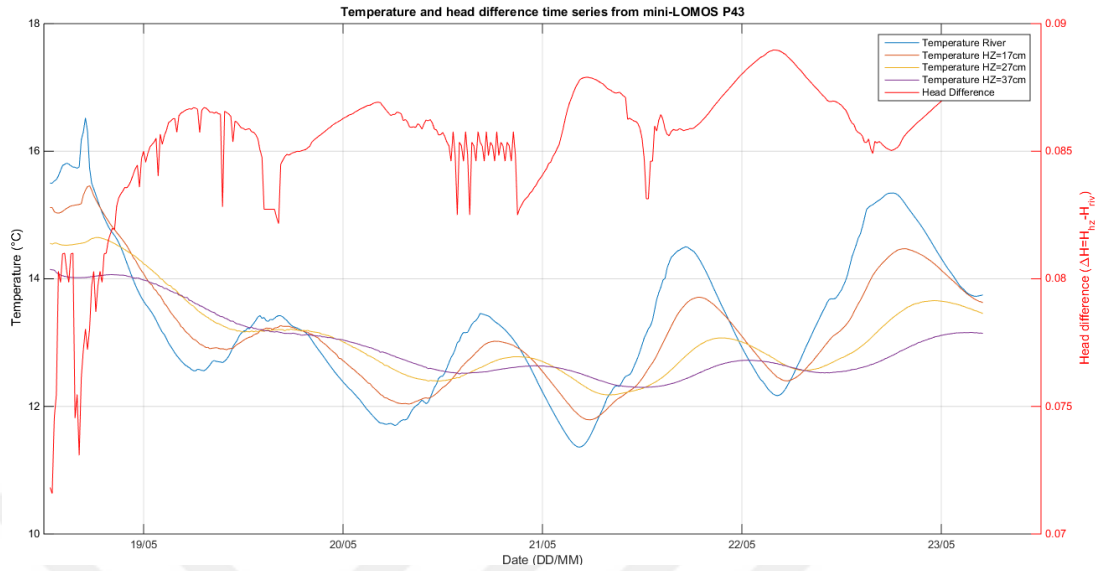

Figure .6: Temperature and head difference time series of mini-LOMOS station P43, this station recorded in Spring season. Red line represents the head difference, and other lines are from each sensor at various depth. The location is at 436 m. The dominant water flux is towards river. The battery failed after 5 days at this position. The temperature sensor at 7 cm did not operate.

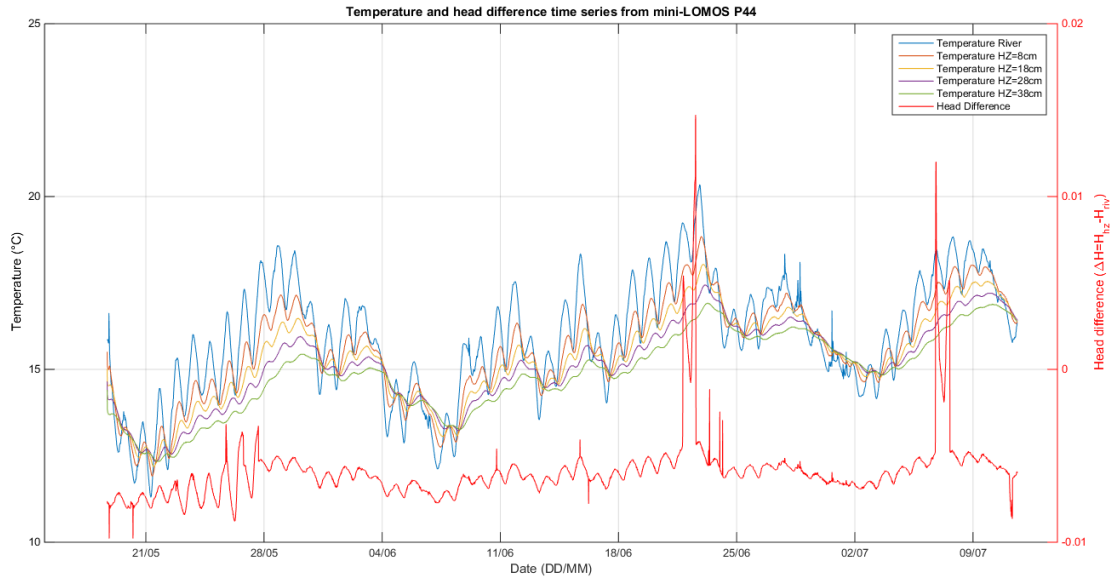

Figure .7: Temperature and head difference time series of mini-LOMOS station P44, this station recorded in Summer season. Red line represents the head difference, and other lines are from each sensor at various depth. The location is at 364 m. The dominant water flux is towards hyporheic zone. There are two small periods with water flux towards river. The sensors are working correctly.

Appendix A continue

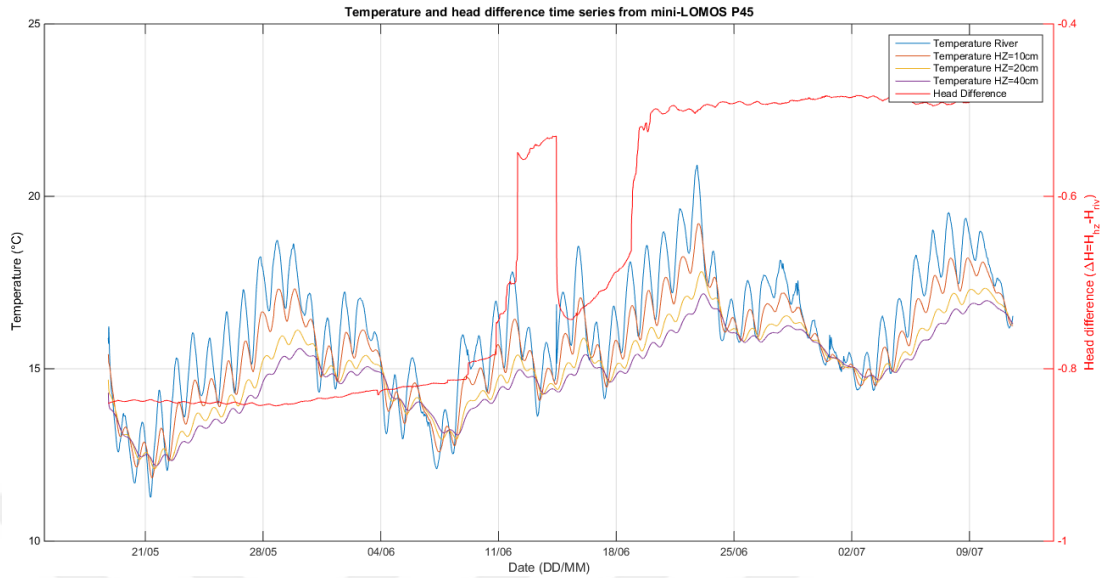

Figure .8: Temperature and head difference time series of mini-LOMOS station P45, this station recorded in Summer season. Red line represents the head difference, and other lines are from each sensor at various depth. The location is at 74 m. The dominant water flux is towards hyporheic zone. The head difference is an order of magnitude higher than other positions. Therefore, one of the pressure sensors might have been damaged. The temperature sensor at 30 cm is damaged, it did not record any data.

Appendix B. Calibration vs observed time series from mini-LOMOS

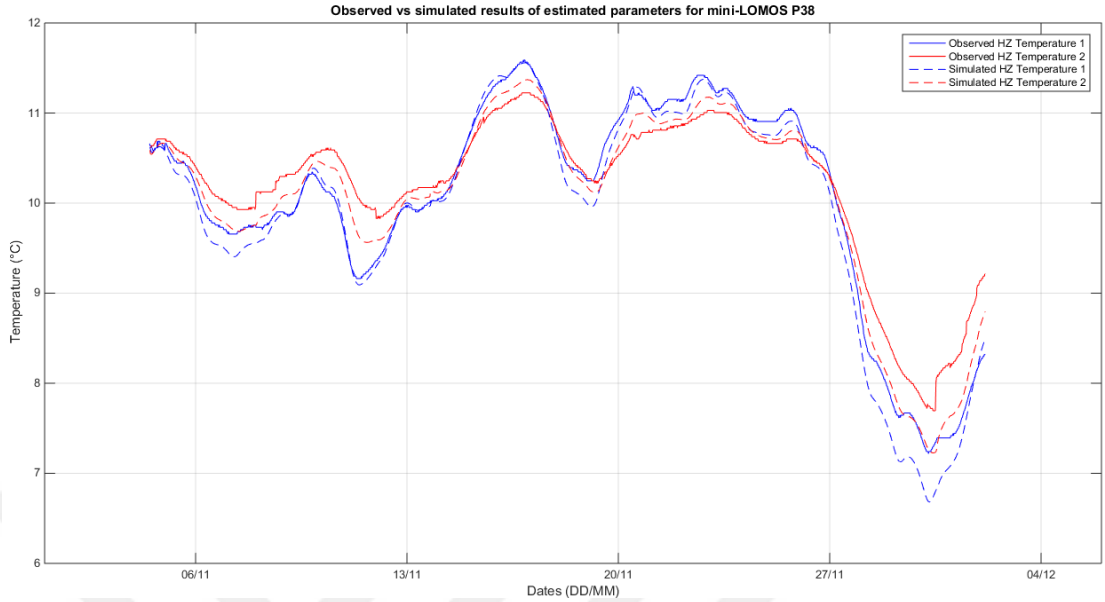

Figure A.1: Simulated vs observed time series for mini-LOMOS station P38. The deepest sensor data was not good for inversion script; thus, it is omitted. The two center sensors are used for calibration. The statistical results of calibration are given in **Error! Reference source not found.**.

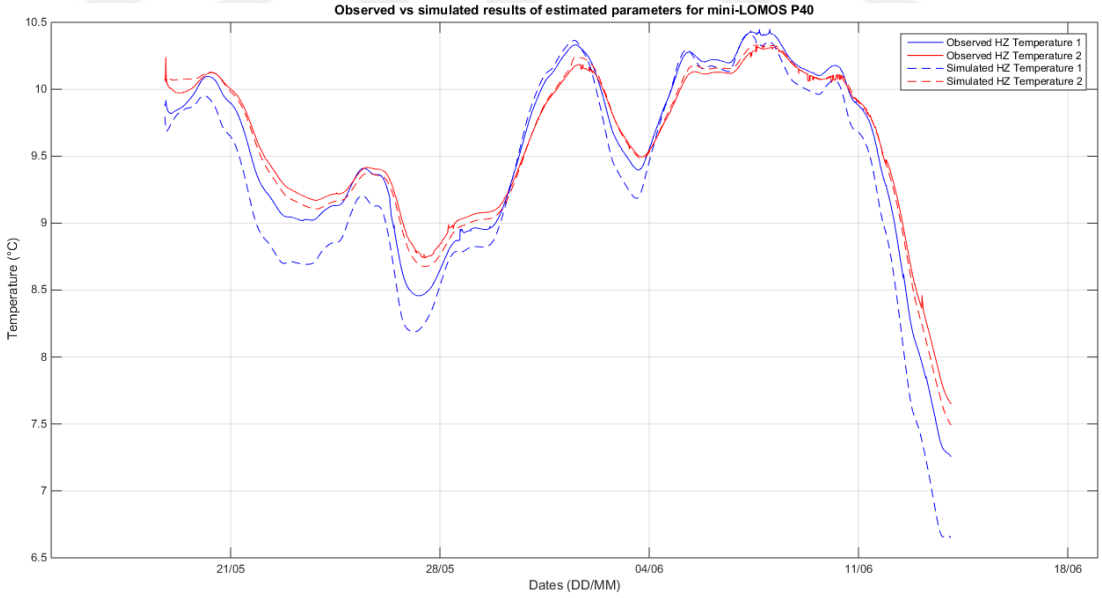

Figure B.2: Simulated vs observed time series for mini-LOMOS station P40. The sensor at 10 cm data was not good for inversion script (observed temperature was 2.5°C higher than other data), thus it is hard to simulate. The other two sensors are used for calibration. The statistical results of calibration are given in **Error! Reference source not found.**.

Appendix B continue

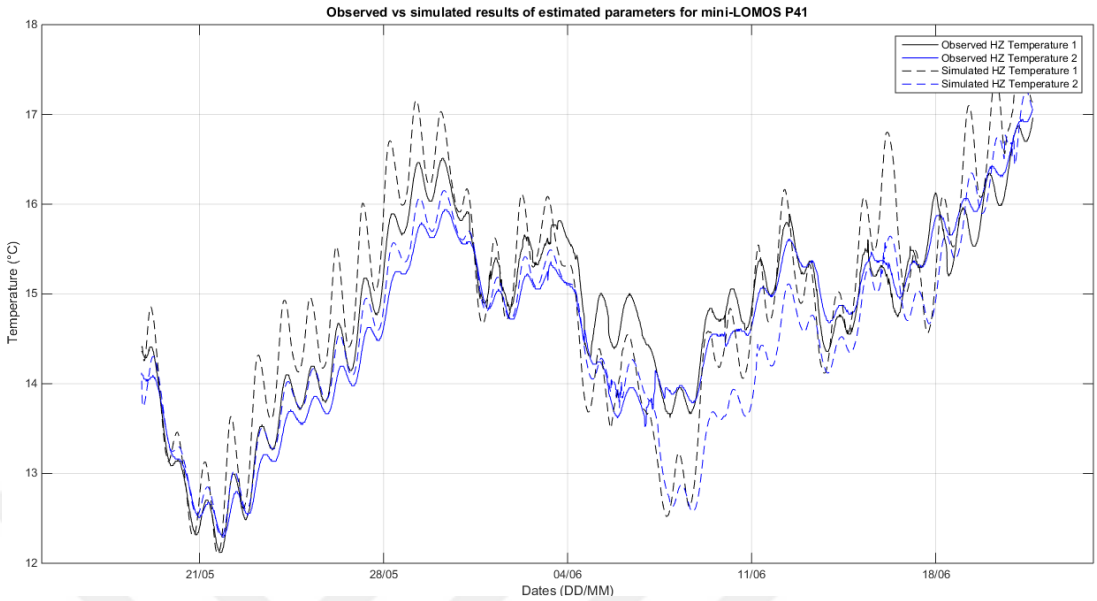

Figure B.3: Simulated vs observed time series for mini-LOMOS station P41. The sensor at 40 cm data was not good for inversion script (the sensor recording is deviating a lot from other sensors); thus, it is hard to simulate. The other two sensors are used for calibration. The statistical results of calibration are given in **Error! Reference source not found.**.

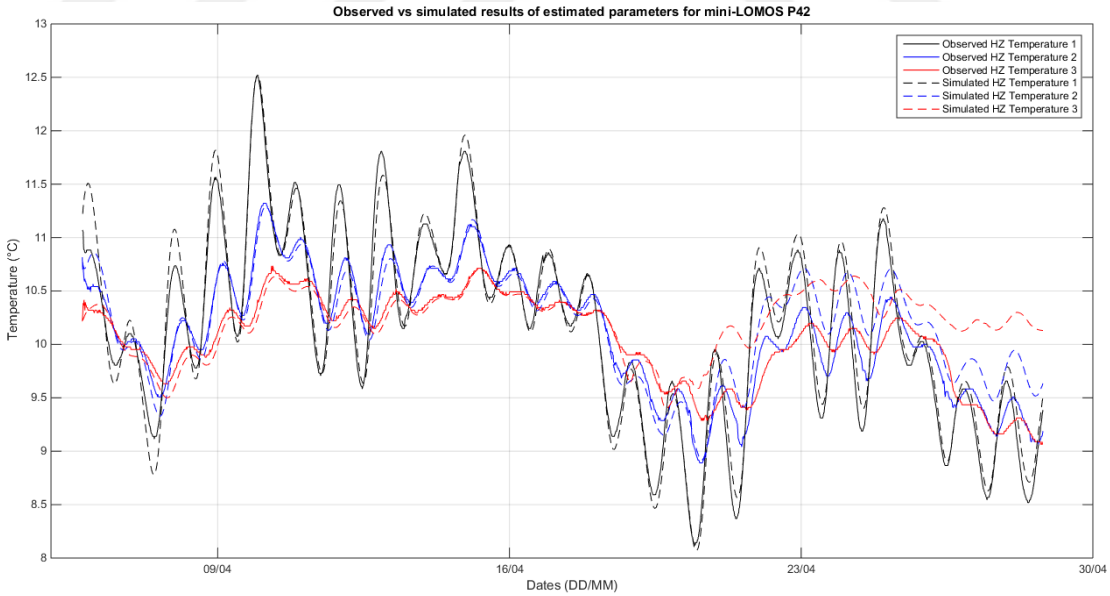

Figure B.4: Simulated vs observed time series for mini-LOMOS station P42. All the temperature sensors are working fine, however, after 20 April, the temperature data recorded at deepest sensor, and the head difference is deviating, thus the simulated temperatures are becoming harder to simulate. The statistical results of calibration are given in **Error! Reference source not found.**.

Appendix B continue

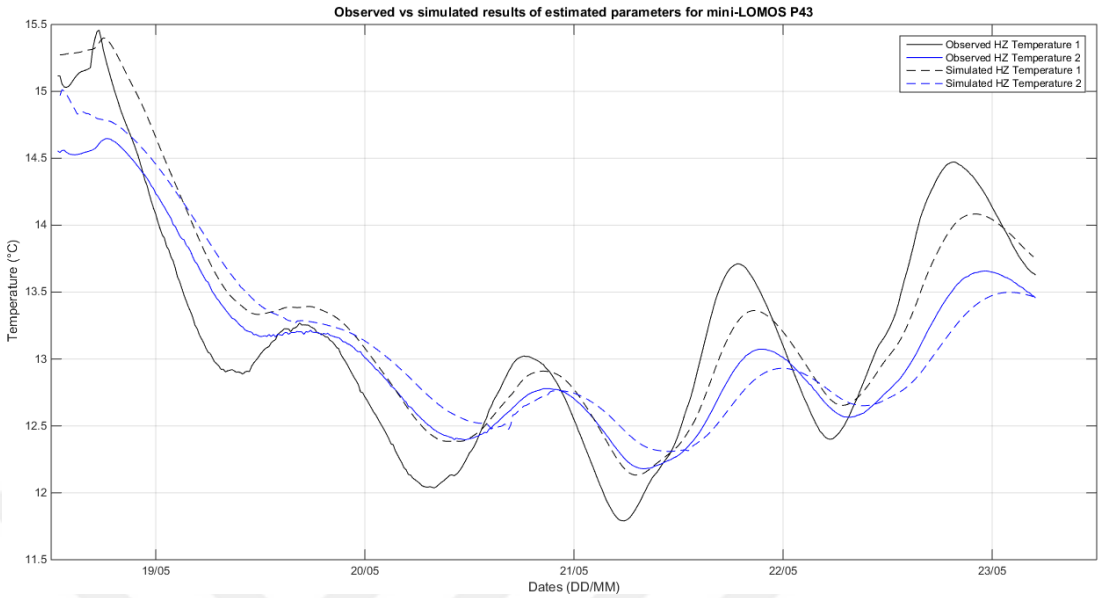

Figure B.5: Simulated vs observed time series for mini-LOMOS station P43. Temperatures are recorded only for 5 days; the sensors are working fine. The statistical results of calibration are given in **Error! Reference source not found.**.

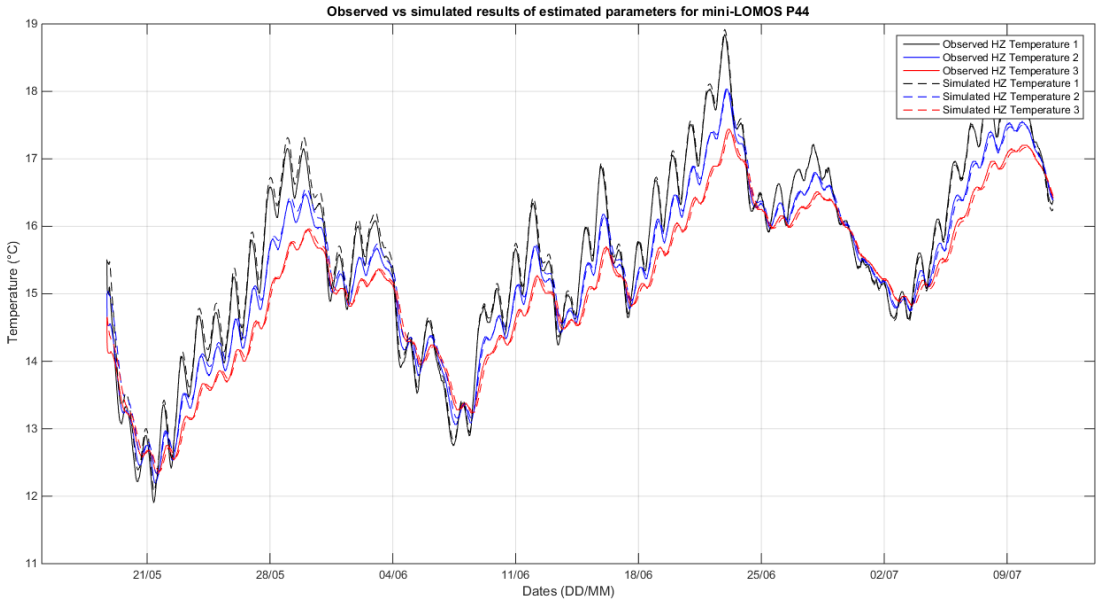

Figure B.6: Simulated vs observed time series for mini-LOMOS station P45. The sensor at 30 cm depth is not working. The calibration is done through other stations. The statistical results of calibration are given in **Error! Reference source not found.**.

Appendix C. Water and heat fluxes from mini-LOMOS

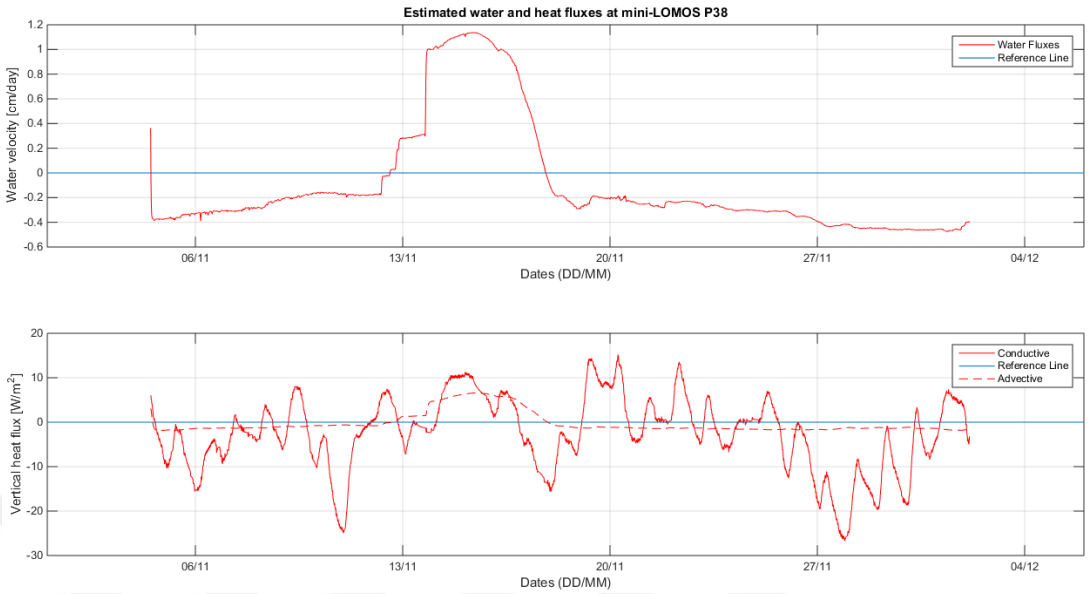

Figure C.1: Estimated fluxes for the mini-LOMOS position P38. The minus sign indicates infiltration.

Appendix C continue

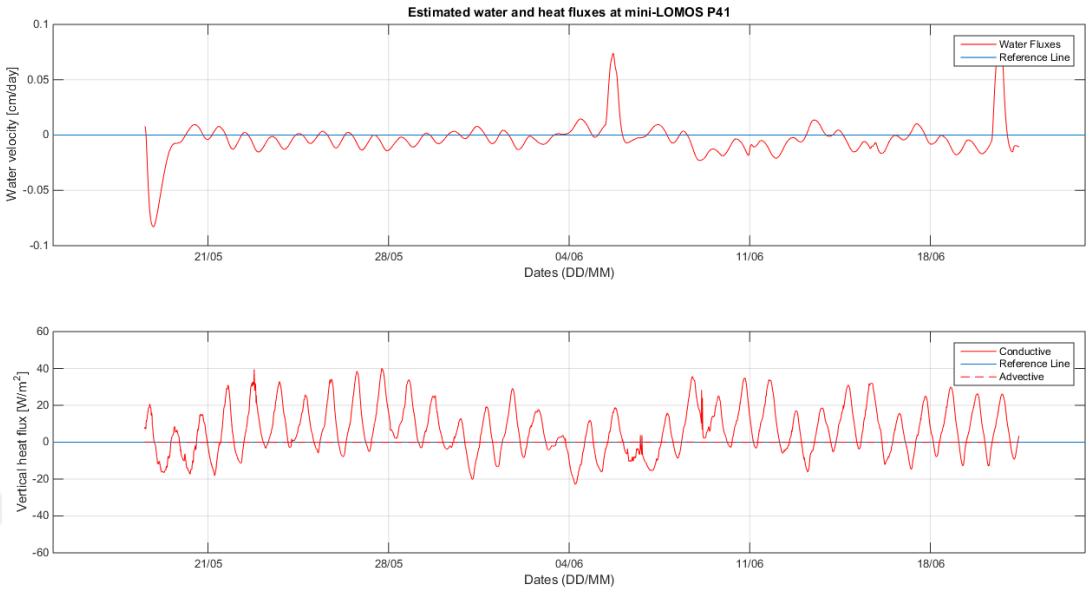

Figure C.2: Estimated fluxes for the mini-LOMOS position P41. The minus sign indicates infiltration.

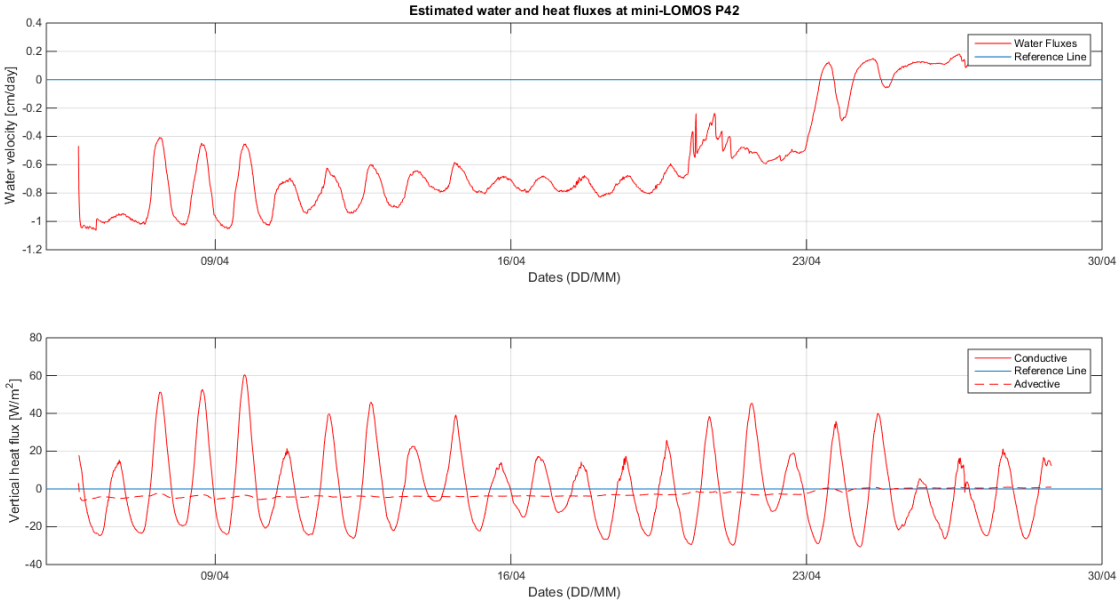

Figure C.3: Estimated fluxes for the mini-LOMOS position P42. The minus sign indicates infiltration. The dominant water flux is towards hyporheic zone. After 23 April the exfiltration is dominant. Conductive heat fluxes have an amplitude of ±25 W/m^2. Advective fluxes are around 5 W/m^2 towards hyporheic zone.

Appendix C continue

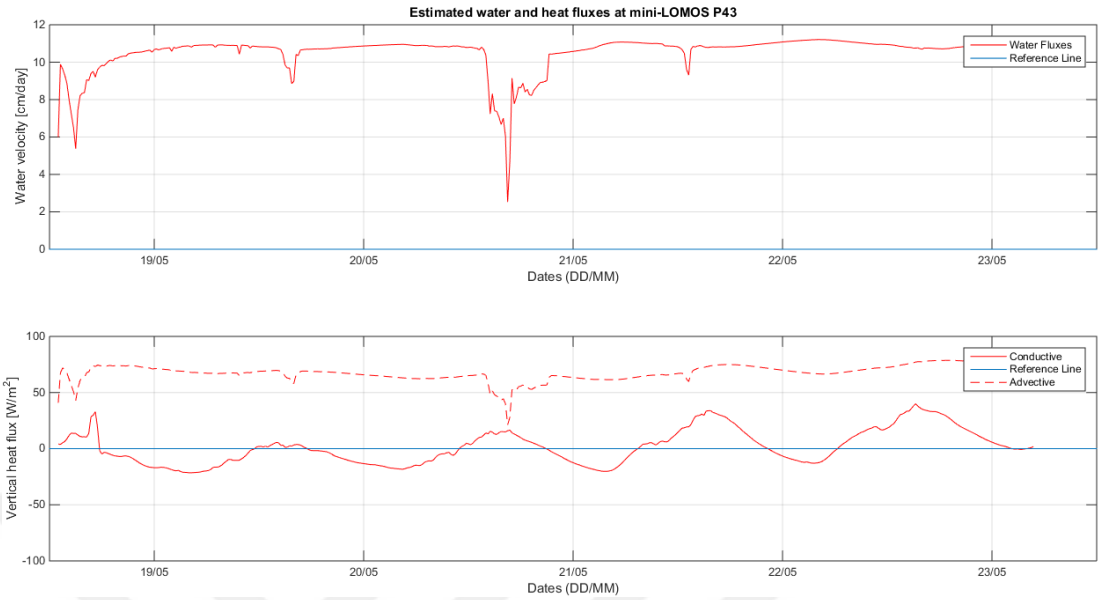

Figure C.4: Estimated fluxes for the mini-LOMOS position P43. The minus sign indicates infiltration.

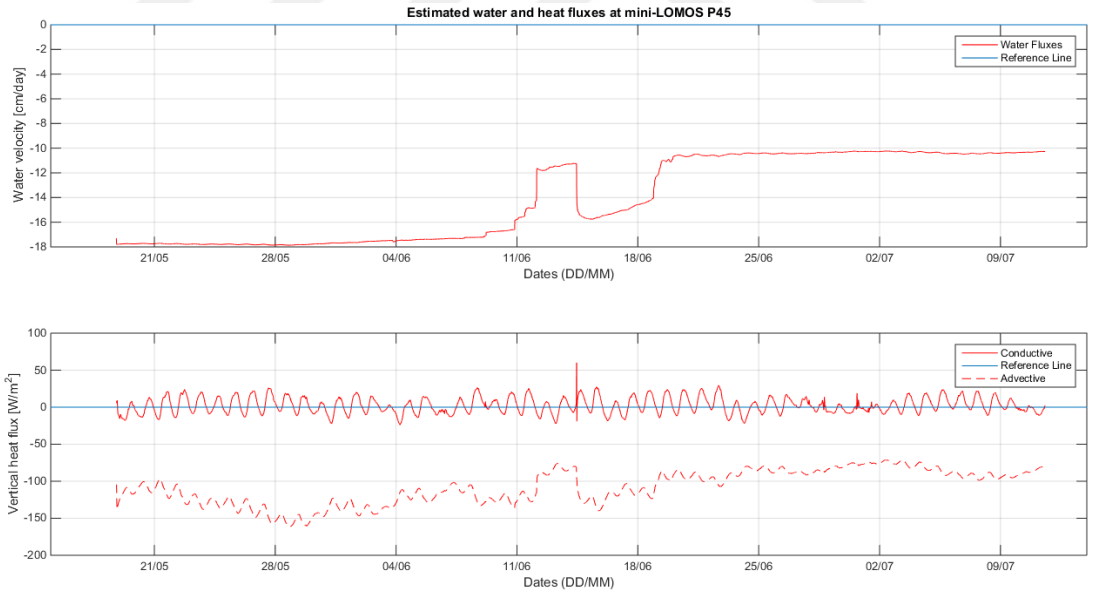

Figure C.5: Estimated fluxes for the mini-LOMOS position P45. The minus sign indicates infiltration. Water fluxes is towards hyporheic zone. This station has much higher water fluxes than other mini-LOMOS stations. The conductive fluxes are ranging between ±30 W/m^2. The dominant advective flux is towards hyporheic zone. Advective fluxes are much higher than conductive fluxes (Ranging between 70-170 ±30 W/m^2).

Appendix D. 2-D model

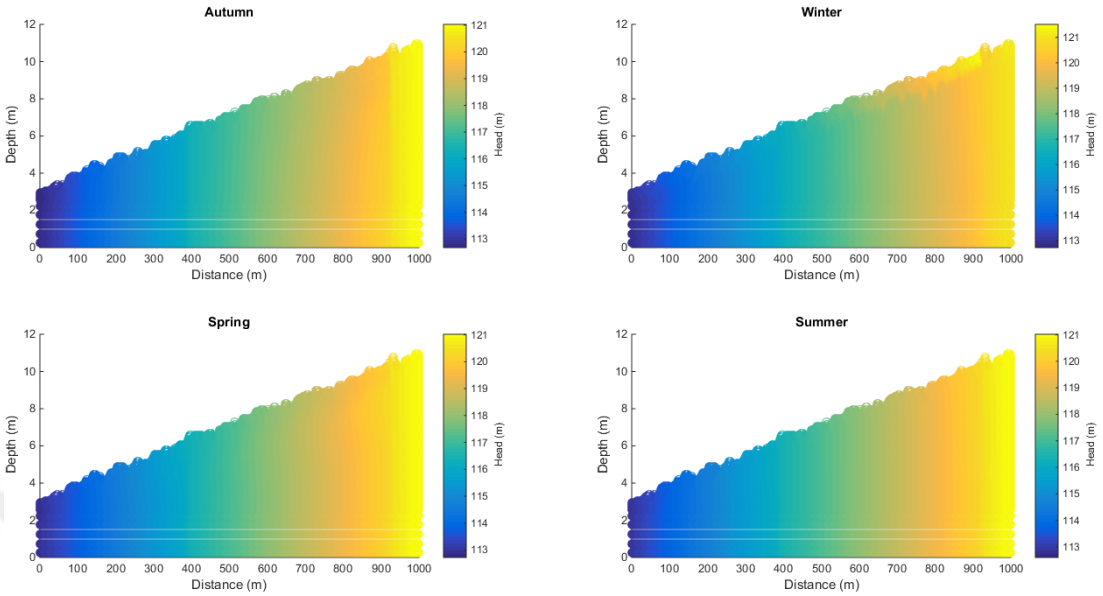

Figure D.1: Seasonal variation of head in 2-D model, a snapshot in time.

CURRICULUM VITAE

Deniz Kılıç
Education

2018 Master of Science in Hydrogeology and associated transfers in University of Poitiers
Poitiers, France

2018 Master of Science in Hydrogeology in Muğla Sıtkı Koçman University
Muğla, Turkey

2016 Bachelor of Science in Geological Engineering in Middle East Technical University
Ankara,Turkey

2015 Erasmus in AGH University of Science and Technology
Krakow, Poland

2010 High School in Edremit Anadolu Lisesi – Balikesir, Turkey

Bachelor's Thesis

Alternative Water Supply Strategies for Burhaniye Town in Balıkesir/Turkey

Work Experience

2.2018-8.2018 Mines ParisTech – Paris, France
Hydrologic Systems and Reservoirs Group
Internship
My work is on spatialization of water-energy exchanges, flux estimation with fiber-optic distributed temperature sensing data and mini Lomos data
Website:<http://www.geosciences.mines-paristech.fr/en/organization/presentation-of-the-group-3>

8.2016-6.2017 ZETAS ATS – Dubai, UAE
Liwa Strategic Water Storage Project
Hydrogeologist
Well Completion Reports, Fluid Flow Tests and Reporting, Well As-Built, Well Composite Logs, Data Processing of 431 wells
Website: <http://www.zetas.com.tr/index.php?id=610000&dil=EN>

6.2013-6.2016 CD-CAT Project – Ankara, Turkey
Student Assistant
Voluntarily assisting professors, doctoral students from Canada, U.S. during field activities, professional interactions, and meetings.
Website: <https://www.esci.umn.edu/orgs/whitney/CD-CAT-index.html>

7-8.2015 Hama Geotechnical Solutions – Ankara, Turkey
Internship
Soil Tests, Slope Stability, Foundation Stability Reports, Offshore Drilling
Website: <http://hamamuhendislik.com/>

7-8.2013 Pars Drilling Solutions – Ankara, Turkey
Internship
PT-PTS Tests and logging, Well Completion, Conventional Drilling, Cored Drilling, Geothermal Systems
Website: <http://www.parsdrilling.com/>

Languages

English – Advanced
French – Basic
Turkish – Mother Tongue

Skills

OS: Linux, Windows
Programs & Languages: Office, ArcGIS, MATLAB, Bash, LaTeX, R, Visual MODFLOW, GeODin, Inkscape, Adobe Illustrator, Adobe Freehand, STANMOD, C, VBA, QGIS, Surfer
Laboratory Experience: Varian Atomic Absorption Spectroscopy, Turner AG-10 Fluorometer, general knowledge on laboratory equipment
Field: Topography surveys, instrument installation such as fiber optic, RBR, Diver etc., water sampling
Other: International Driver's Licence – A2/B, Experience with small size boats in lakes for surveys etc.

Member of

English Conversation Class – Maison des Langues, Poitiers – 2017
AFEV – Poitiers - 2017
American Association for the Advancement of Science – 2017
Society of Economic Geology – METU Student Chapter (Founding Member, Treasurer) - 2016
Society of Geology in METU – 2012
METU Rowing Team - 2011

Scholarships

9.2017-9.2018 Joint Scholarship of Government of France and SKV Foundation

Interests

Hiking, Cycling, Rowing, Tennis